ISSN: 2153-1196 Volume 10, Number 4, March 2019

Scientific Research Publishing

Journal of Modern Physics

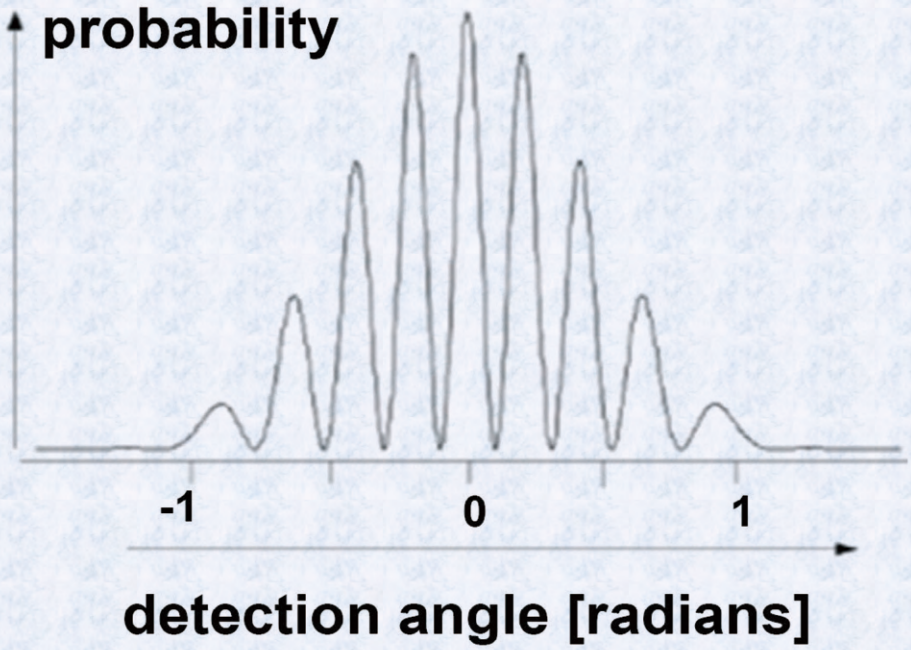

ISSN: 2153-1196
9 772153 119007 04

www.scirp.org/journal/jmp

Journal Editorial Board

ISSN: 2153-1196 (Print) ISSN: 2153-120X (Online)
http://www.scirp.org/journal/jmp

Editor-in-Chief

Editorial Board

Scientific Research Publishing

Journal of Modern Physics, 2019, 10, 423-485
http://www.scirp.org/journal/jmp
ISSN Online: 2153-120X
ISSN Print: 2153-1196

Table of Contents

Volume 10 Number 4 March 2019

The figure on the front cover is from the article published in Journal of Modern Physics, 2019, Vol. 10, No. 4, pp. 423-431 by Arend Niehaus.

Journal of Modern Physics (JMP)
Journal Information

SUBSCRIPTIONS

The *Journal of Modern Physics* (Online at Scientific Research Publishing, www.SciRP.org) is published monthly by Scientific Research Publishing, Inc., USA.

Subscription rates:
Print: $89 per issue.
To subscribe, please contact Journals Subscriptions Department, E-mail: sub@scirp.org

SERVICES

Advertisements
Advertisement Sales Department, E-mail: service@scirp.org

Reprints (minimum quantity 100 copies)
Reprints Co-ordinator, Scientific Research Publishing, Inc., USA.
E-mail: sub@scirp.org

COPYRIGHT

PRODUCTION INFORMATION

For manuscripts that have been accepted for publication, please contact:
E-mail: jmp@scirp.org

Journal of Modern Physics, 2019, 10, 423-431
http://www.scirp.org/journal/jmp
ISSN Online: 2153-120X
ISSN Print: 2153-1196

Quantum Interference without Quantum Mechanics

Arend Niehaus*

Utrecht University, Utrecht, The Netherlands
Email: arendniehaus@aol.com

How to cite this paper: Niehaus, A. (2019) Quantum Interference without Quantum Mechanics. *Journal of Modern Physics*, **10**, 423-431.
https://doi.org/10.4236/jmp.2019.104027

Received: February 9, 2019
Accepted: March 16, 2019
Published: March 19, 2019

Abstract

A recently proposed model of the Dirac electron, which has been shown to describe several observed properties of the particle correctly, is in the present paper shown to be also able to explain quantum interference by classical probabilities. According to this model, the electron is not point-like, but rather an "entity with structure", formed by a fast periodic motion of a "light-like object", whose momentum (p) causes the angular momentum responsible for the spin, and whose energy ($E = pc$) is equal to the energy of the electron, mc^2. A qualitative description of the model is given, together with the quantitative formulae that allow to discuss interference. Applied to the experimental situation of the "two-slit" experiment, the formulae yield the same time dependence of the detection probability as the quantum mechanical treatment, and hence the same interference pattern. In contrast to quantum mechanics, the pattern is due to "particle interference" rather than to "wave interference". No wave-particle paradox arises. The merits of the model are summarized, and its physical content discussed.

Keywords

Interpretation of Quantum Mechanics, Quantum Interference, Classical Probability

1. Introduction

Quantum mechanics treats the electron as a point-like particle having a certain mass, but no structure. To describe observed phenomena correctly, it ascribes certain other properties to the particle, for instance spin, and a wavelike nature, which are "non-classical", and cannot be "derived" (e.g. [1]). The validity of the theory is unquestioned; however, its interpretation is still subject of debate (see, f.i., [2]), because the "quantum world" it creates contains numerous well known paradoxes.

*Retired Professor of Physics.

There have been attempts to escape interpretational problems by supposing that the electron, and possibly other elementary particles also, do have an internal structure that possibly could explain their properties. Especially, the fact that a so called "Zitterbewegung (ZBW)" [3] is one of the properties arising from the relativistic quantum theoretical treatment of the free electron, has led to the proposal of a dynamic substructure [4] [5] [6]. Typical time scale for such a structure would be the very short period (τ) of the (ZBW):

$\tau = 2\pi/\omega_{ZBW}$ with $\omega_{ZBW} = 2c/L_0$, leading to $\tau = 2\pi L_0/2c \approx 4{\cdot}10^{-21}$ s.

Theoretical analyses have indeed shown that the spin, arising in the Dirac theory, can be related to a motion; however, an *extended* (ZBW), not predicted by the Dirac theory, would be necessary to explain the properties of the electron [6]. Also *models* of the electron, based on the (ZBW), have been proposed [7] [8]. For a recent discussion we refer to [9].

The model to be used in this paper, is also based on the assumption of a (ZBW). But the new aspect is that, the (ZBW) is not ascribed to the electron, but rather to a light-like object that possesses momentum and energy, and establishes the electron by its periodic motion around a point in space. The model has been developed in two recent publications [10] [11][1] of the present author, and has been shown to explain the properties like spin, magnetic moment, and mass, of the electron. In the present paper it will be shown to be also able to explain quantum interference using classical probabilities. First, we give a short qualitative description of the model.

Starting from the assumption that spin is caused by orbital motion due to an *extended* (ZBW), a probability distribution of orientation and value of an *instantaneous orbital angular momentum* is designed, which describes spin and spin measurements in accordance with experiment. Under the assumption that the "object" that causes the angular momenta is "light-like", with momentum ($p = \hbar/L$), probability distributions for orientation and length of the *instantaneous position vector* of the "light-like object", which we will call "quantum", are derived from the angular distributions. The instantaneous *positions* of the quantum turn out to lie on a torus around a fixed point, the torus radius (R_t) being equal to the radius of the circle (R_c) the torus axis forms around the fixed point: $R_t = R_c = (L/2)$. This special Torus is a so called Clifford Torus. The relation between instantaneous position vector ($\boldsymbol{r}$) of the quantum, its instantaneous momentum ($\boldsymbol{p}$), and the resulting instantaneous angular momentum vector ($\boldsymbol{I} = \boldsymbol{r} \times \boldsymbol{p}$) is depicted in **Figure 1**.

The Torus, on whose surface the instantaneous positions of the quantum are located, is shown in **Figure 2**.

In Cartesian coordinates the position vector is given by

$$r(x,y,z) = L\left\{\cos^2(\theta)\cos(\varphi), \cos^2(\theta)\sin(\varphi), \sin(\theta)\cos(\theta)\right\} \qquad (1)$$

The idea is now, to describe the distributions in terms of the extended ZBW of

[1]Erroneously, the labels (a) and (b) of the two figures in **Figure 3** were interchanged in the final typesetting.

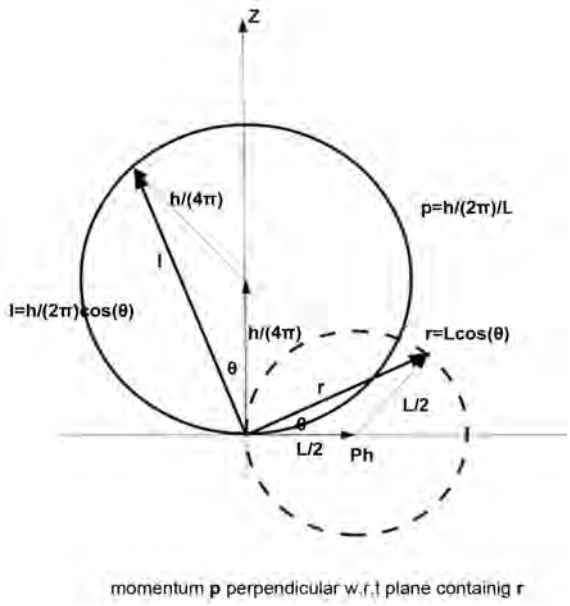

Figure 1. Relation between the following instantaneous vectors, 1) momentum ($\boldsymbol{p}$) of the quantum, 2) its position ($\boldsymbol{r}$), and 3) of the resulting angular momentum $\boldsymbol{I} = \boldsymbol{r} \times \boldsymbol{p}$. Equal population of the circle around the point **Ph** by the quantum, together with cylindrical symmetry around the Z-axis, lead to the required angular distribution $I(\theta) = (h/2\pi)\cos(\theta)$, which explains spin and spin measurements correctly (see Ref. [10]).

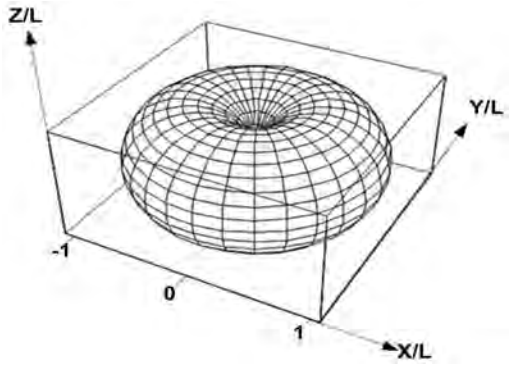

Figure 2. The instantaneous positions of the quantum are located on the surface of a Clifford Torus. The torus radius (R_t) is equal to the radius of the circle (R_c) the torus axis forms around the fixed point: $R_t = R_c = L/2$.

the quantum. To obtain a motion of the quantum on the torus surface, we relate the angles (θ, ϕ) as

$$\varphi = \omega_p t; \theta = \left(\frac{\omega_t}{2}\right) t; \omega_p = n\omega_t \tag{2}$$

The parameter (t) is taken to be proper time, so that (ω_p, ω_t) are frequencies, and the position vector describes a path in space and time on the surface of the

torus. From (1) we get:

$$r(x,y,z,t) = L\left\{\cos^2\left(\left(\frac{\omega_t}{2}\right)t\right)\cos(\omega_p t), \cos^2\left(\left(\frac{\omega_t}{2}\right)t\right)\sin(\omega_p t), \frac{\sin(\omega_t t)}{2}\right\} \quad (3)$$

As an example, we show in Figure 3 the path for the case $n = 10$ as calculated with (3).

Properties of the "entity" obtained using relation (3) as averages over an observation time, approach definite values after times sufficiently long compared to the period $\tau = 4\pi/\omega_t$. If (L) is taken to be the reduced Compton wavelength $L = \hbar/mc$, with (m) the relativistic mass of the particle described, such values are, for instance, spin = $\hbar/2$, and the correct magnetic moment = $\hbar e/(2m_0)$. We stress that the value of the number (n) has no influence on the general situation described so far.

We identify the "entity", if it is observed with a sufficiently low time-resolution, with the particle described. Then, the center of the torus is the position of the particle, and due to the dynamical origin of its torus-structure, it has its established properties.

In this paper we attempt to describe the property "wave nature" of moving particles. It becomes observable by the phenomenon *interference*, for instance in the two-slit experiment. Therefore, the velocity (v) is introduced into the model represented so far by relation (3). Assuming a velocity in Z-direction, this is done in the following way:

1) The coordinate (z) is replaced by $(z+vt)$; 2) $L = L_0\left(1-\beta^2\right)^{1/2}$ with $\beta = v/c$; 3) $\omega_p = 2c/L_0$ so that ω_p becomes the ZBW-frequency arising in the Dirac theory.

The velocity component at the torus axis (at point **Ph** in Figure 1) in the X-Y plane thus becomes $\omega_p L/2 = c\left(1-\beta^2\right)^{1/2}$, and the velocity component in Z-direction is (βc), resulting in a constant tangential speed (c) at the torus axis,

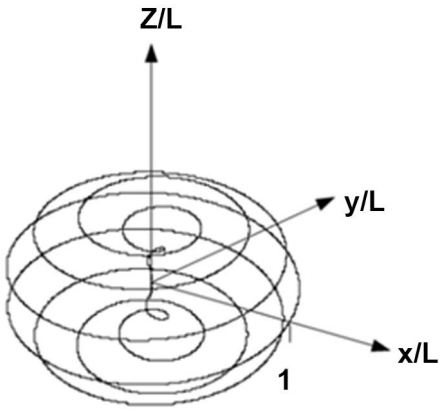

Figure 3. The closed path of the quantum. The "entity" it forms is taken to represent the electron for the case ($\omega_p/\omega_t = n = 10$). Coordinates are given in units of the reduced Compton wave length (L). The path lies on the surface of the Torus shown in Figure 2.

independent of (v), as required. The ratio of the frequencies becomes: $\omega_p/\omega_t = n = \left(1-\beta^2\right)^{1/2}/\beta$, so that $\beta = 1/\left(1+n^2\right)^{1/2}$.

The complete model for the case of a velocity ($v = \beta c$) in Z-direction may thus be represented by the modified relation (3) as follows:

$$r(x,y,z,t,\beta) = L_0 n\beta\left\{\cos^2\left(\left(\frac{\omega_t}{2}\right)t\right)\cos\left(\omega_p t\right), \cos^2\left(\left(\frac{\omega_t}{2}\right)t\right)\sin\left(\omega_p t\right), \frac{\sin\left(\omega_t t\right)}{2} + \frac{ct}{nL_0}\right\}$$

$$L_0 = \frac{\hbar}{m_0 c}; \omega_p = \frac{2c}{L_0}; \omega_t = \frac{\omega_p}{n}; n = \left(1-\beta^2\right)^{1/2}/\beta; \quad (4)$$

The model is completely general and contains no free parameters. In this paper we will demonstrate, in which way it describes observed interference phenomena of electrons correctly. As example we discuss the two slit experiment in paragraph (2).

2. Interference

First we show in **Figure 4** a 3D-parametric plot of the path of the quantum during a time span of 2.5 periods $\left(\tau = 4\pi/\omega_t\right)$ for the case n = 10, as calculated using relation (4).

In order to treat interference in the two-slit experiment, we need the velocity of the quantum in Z-direction (vq). As calculated using (4), this velocity is given by

$$vq = 2v\cos^2\left(\frac{\omega_t}{2}\right) = 2v\cos^2\left(\omega_{DB}t\right) \quad (5)$$

where, according to the definition of the Torus frequency given in (4), ω_{DB} is the De Broglie frequency defined as $\omega_{DB} = c/L_{DB} = c\,\mathrm{mv}/\hbar$.

For the case of many particles starting with a different phase (φ) from a certain position in Z-direction, there arises a constant current of quanta in Z-direction, which is obtained by integration over (φ). Assuming equal probability ($1/2\pi$) for different phases, the current becomes

$$I(t) = \left(\frac{1}{2\pi}\right)\int_0^{2\pi} 2v\cos^2\left(\omega_{DB}t+\varphi\right)\mathrm{d}\varphi = v \quad (6)$$

Let us now consider the normal two-slit situation in the context of the model, where diffracted particles from the two narrow slits separated by distance (B) form currents into certain directions behind the slits, and hit the surface of a screen that is oriented perpendicular to the currents and positioned at a distance large compared to the distance between the two slits (see **Figure 5**).

Then, at any position on the screen determined by the diffraction angle ($+\delta$), particles from both slits will arrive. For symmetry reasons, the same current will arrive at the angle ($-\delta$). For each particle detected at ($+\delta$) on the screen at time (t), there is a certain probability that it originates from slit 1, or slit 2. According to classical probability theory [12], this *conditional probability* is obtained by the unification of the probabilities for the two slits, P1 and P2.

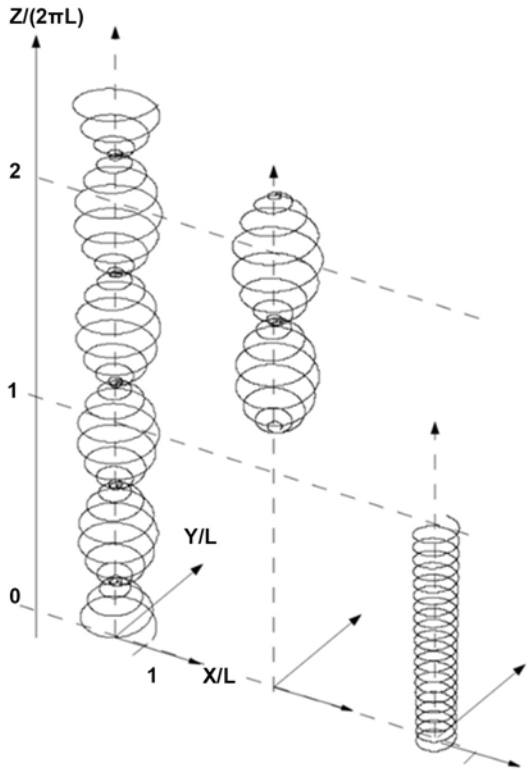

Figure 4. Traces from left to right: 1), A parametric 3D plot of the positions in real space of the quantum (in units of L) during the first 2.5 periods of the (EZBW), for the case $n = 10$. 2), Path of the quantum during one period, starting 1.3 periods after ($t = 0$). 3), Path of the point (**Ph**) on the torus axis (see **Figure 1**) during the first period. Its tangential speed is (c) (see text). Progress of the "entity" in z-direction is seen to proceed at the velocity $v = 2\pi L/\tau = \beta c$, while progress of the quantum is given by $vq = 2v\cos^2\left((\omega_t/2)t\right)$ (see text).

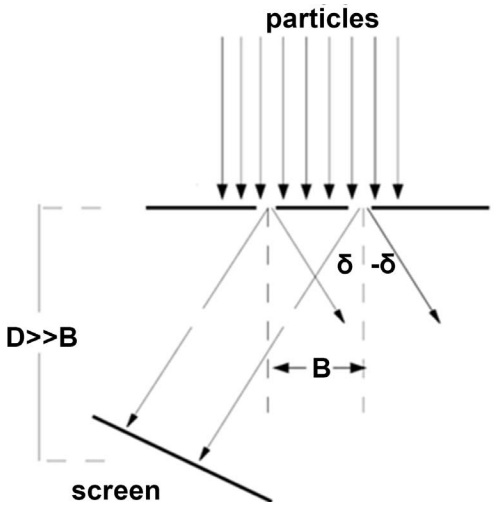

Figure 5. The two slit situation. The distance (D) of the screen from the slits is large compared to the distance (B) between the slits.

$$P(t,\varphi,+\delta)=(P1 \text{ or } P2)=P1+P2-P1\cap P2 \tag{7}$$

The last term in (7) is the intersection between the probabilities $P1$ and $P2$. Using relation (5), and setting the constant current to $v=1$, we have $P1=2\cos^2(\omega_{DB}t+\varphi)$ and $P2=2\cos^2(\omega_{DB}(t+Dt)+\varphi)$. The intersection is the probability that both paths—via slit 1, and via slit two—lead to detection at $(-\delta)$. In the present case, we identify the intersection as $P1\cap P2=\left(\cos(\omega_{DB}t+\varphi)-\cos(\omega_{DB}(t+Dt))+\varphi\right)^2$. The total probability on the screen at position (+δ) is then obtained by integration of (7) over possible initial conditions (φ):

$$\begin{aligned}&P(t,+\delta)\\&=\int_0^{2\pi}\left\{2\cos^2(\omega_{DB}t+\varphi)+2\cos^2(\omega_{DB}(t+Dt)+\varphi)\right.\\&\quad\left.-\left(\cos(\omega_{DB}t+\varphi)-\cos(\omega_{DB}(t+Dt)+\varphi)\right)^2\right\}\mathrm{d}\varphi\\&=2\cos^2\left(\frac{\omega_{DB}Dt}{2}\right)\end{aligned} \tag{8}$$

As is well known, the probability given by (8), is identical to the probability calculated in quantum mechanics for the superposition (Ψ) of two equal amplitude, single momentum, particle De Broglie waves, starting from the two slits. This is indicated below.

$$\Psi=\left(1/\sqrt{2}\right)\left(\mathrm{e}^{ikr}+\mathrm{e}^{ik'r}\right);\Psi\Psi^*=2\cos^2\left(\frac{k(r-r')}{2}\right)=2\cos^2\left(\frac{\omega_{DB}Dt}{2}\right) \tag{9}$$

In (9) we used the De Broglie wavenumber $k=1/L_{DB}=\omega_{DB}/c$, and the fact that $(r-r')=cDt$, the extra distance to be travelled from the more distant of the two slits.

The different derivations, (8) and (9), of the same result, clearly show the relation between model and quantum mechanics for the case of interference. Most remarkably, the non-local wave nature, ascribed in the quantum mechanical description to a single particle, the model ascribes to an *ensemble* of localized particles having a certain structure. Therefore, the paradoxical wave-particle dualism does not arise.

Below we demonstrate the prediction of a two-slit interference pattern using result (8) for a concrete case. The dependence of the detection probability on the angle (δ), for a given $v=\beta c$, is given through the relations $S=cDt=B\sin\delta$, and $L_{DB}=L/\beta=L_0\sqrt{(1-\beta^2)}/\beta=L_0 n$, so that the phase in (8) becomes $S/2L_{DB}=B\sin\delta/2nL_0=\pi(B/\lambda_{DB})\sin\delta$.

Relation (8) is the predicted interference pattern for the case of two infinitely narrow slits separated by a distance (B). In a realistic case, the slits have a finite width (d), so that interference of particles coming from different positions *within* one slit arises, and leads to a certain single-slit interference pattern, which can be calculated approximately with relation (8) by replacing (B) by $(d/2)$. At sufficiently narrow slit widths (d), and a slit distance (B) considerably larger than (d), the complete interference pattern thus becomes a modulation of the diffraction

profile by the two-slit interference. In Figure 6 we show an example using $B/\lambda_{DB} = 5$ to calculate the two slit modulation, and $d = \lambda_{DB}$ to calculate the diffraction profile. At this width we have $d = \Delta x = \lambda_{DB}$, and a width of the diffraction peak corresponding to $\Delta p = p = \hbar/\lambda_{DB}$, so that the uncertainty relation inherent in the model becomes $\Delta p \Delta x = \hbar$.

As the main result of the present paper we state that the two-slit quantum interference is correctly described without quantum mechanics.

3. Conclusion and Discussion

The dynamic substructure, which the model ascribes to the particle, explains the two slit interference, one of the main quantum phenomena, without using quantum mechanics. In a similar way, energy quantization of bound states, as well as angular momentum quantization, is predicted by the model in agreement with observation. In addition, as has been shown in the previous papers [10] [11], the properties of the electron, mass, spin, and magnetic moment, follow from the substructure implied by the model. Further, the paradox of "wave-particle dualism" does not arise, because "wave interference" is explained as "particle interference".

As already mentioned, the model is based on the idea that spin might be explained as angular momentum caused by a quantum of momentum (mc) when it passes a fixed point in space. The *completed* model of an elementary particle, used in this paper, may be visualized in a very simple way: The point (**Ph**) (see Figure 1), which is located in the center of the circle containing the quantum, is identified as a *photon*, and the point, which is located in the center of this circulating photon, is identified as the *particle*. As shown in Figure 4, the photon forms a spiraling trace with tangential speed (c), independent of the relative motion (v) with respect to an observer, and its energy is $pc = mc^2$, with $\left(m = m_0 \big/ \sqrt{\left(1-\beta^2\right)}\right)$. The momentum *component* of the photon in direction of relative motion, $\left(mv = m\beta c = m_0 c/n\right)$, is the momentum of the "particle".

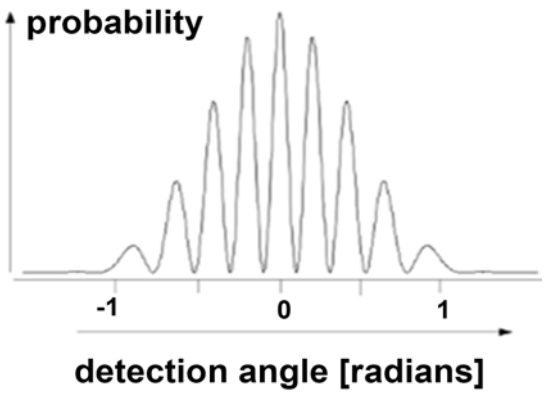

Figure 6. The two slit interference pattern for "particles" calculated with formula (8).The central diffraction peak, common to both slits, is modulated by the two-slit interference. The same interference pattern would be calculated using quantum mechanics.

There remain important questions regarding the validity of the model. On the other hand, in our opinion, its demonstrated successes are too manifold and substantial to be accidental. Therefore, a thorough theoretical investigation of the model, especially of its relation to quantum field theory, seems interesting.

Conflicts of Interest

The author declares no conflicts of interest regarding the publication of this paper.

References

[1] Messiah, A. (1964) Quantum Mechanics. Vol. II, North Holland Publishing Company, Amsterdam, 540.

[2] Khrennikov, A. (2017) *Foundations of Physics*, **47**, 1077-1099. https://doi.org/10.1007/s10701-017-0089-0

[3] Schroedinger, E. (1930) *Sitzungsber. Preuss. Akad. Wiss. Phys.-Math. Kl.*, **24**, 418.

[4] Hestenes, D. (1979) *American Journal of Physics*, **47**, 399-415. https://doi.org/10.1119/1.11806

[5] Hestenes, D. (1990) *Foundations of Physics*, **20**, 1213-1232. https://doi.org/10.1007/BF01889466

[6] Hestenes, D. (2003) *Annales de la Fondation Louis de Broglie*, **28**, 390-408.

[7] Barut, A.O. and Sanghi, N. (1984) *Physical Review Letters*, **52**, 2009-2012. https://doi.org/10.1103/PhysRevLett.52.2009

[8] Vaz Jr., J. (1995) *Physics Letters B*, **344**, 149-157. https://doi.org/10.1016/0370-2693(94)01548-Q

[9] Pavsic, M., Recami, E., Waldyr, A., Rodriges Jr., G., Maccarrone, D., Racciti, F. and Salesi, G. (1993) *Physics Letters B*, **318**, 481-488. https://doi.org/10.1016/0370-2693(93)91543-V

[10] Niehaus, A. (2016) *Foundations of Physics*, **46**, 3-13. https://doi.org/10.1007/s10701-015-9953-y

[11] Niehaus, A. (2017) *Journal of Modern Physics*, **8**, 511-521. https://doi.org/10.4236/jmp.2017.84033

[12] Bauer, H. (2002) Wahrscheinlichkeitstheorie. De Gruyter, Berlin, New York.

Journal of Modern Physics, 2019, 10, 432-442
http://www.scirp.org/journal/jmp
ISSN Online: 2153-120X
ISSN Print: 2153-1196

Disorder Effect on the Transmission of Second Harmonic Waves in One-Dimensional Periodically Poled $LiTaO_3$

Bahrami Omid*, Baharvand Abdolrahim, Bahari Ali

Department of Physics, Faculty of Science, Lorestan University, Khorram-Abad, Iran
Email: *bahrami.om@fs.lu.ac.ir

How to cite this paper: Omid, B., Abdolrahim, B. and Ali, B. (2019) Disorder Effect on the Transmission of Second Harmonic Waves in One-Dimensional Periodically Poled $LiTaO_3$. *Journal of Modern Physics*, **10**, 432-442.
https://doi.org/10.4236/jmp.2019.104028

Received: February 19, 2019
Accepted: March 16, 2019
Published: March 19, 2019

Abstract

One of the methods for calculating electromagnetic wave dispersion in multi-layer structures is the transfer matrix method. In this paper, we use the transfer matrix method for second harmonic generation in a nonlinear multilayer structure. The nonlinear photonic crystals investigated in this paper are as one-dimensional multi-layered structures including ferroelectric materials such as $LiTaO_3$. Our goal is to investigate the effect of the disorder on the transmission spectrum of electromagnetic waves. Our results showed that positional disorder has different effects on the transmitting band and the gap band. The disorder in the transmitting band reduces the transmission coefficient of the waves and increases the transmission coefficient of the waves in the gap band. Such work has not yet been done on nonlinear photonic crystals producing the second harmonic.

Keywords

Transfer Matrix Method, Nonlinear Photonic Crystal, Random Binary Medium, Transmission Spectra, Disorder Effect, Second Harmonic Waves

1. Introduction

In recent decades, the study of the transmission of waves in random systems has been highly studied because it plays an important role in understanding the optical, mechanical, magnetic, and electrical properties of materials. The most important theory in this case is Anderson's theory. This theory is about electrons crossing in random systems [1] [2]. Although Anderson's theory was initially about the transmission of electron waves in disordered systems, it was later extended to other waves such as electromagnetic and acoustic waves.

A weak disorder in 3D devices does not turn all of the extended modes into localized modes. That is; there is a series of transmission modes in the system. For strong disorder, due to the incoherent interference of waves, transmitted modes are exponentially localized. For one-dimensional systems, Anderson's theory shows that all the passing modes are exponentially localized for any degree of disorder [2] [3].

There are several models for one dimensional multi-layer system in which exponential localization is violated. For example a one-dimensional system with the periodic period consisting of two parts is known as a random-dimer model [4] [5]. In this type of system, there are modes that disorder does not affect them. Another model that violates Anderson's localization in disordered one-dimensional systems is a long-range correlation model [6] [7]. The tight-binding 1D model also violates the exponential localization in one-dimensional systems that occur for any disorder [8] [9]. Finally, the last model that produces non-localized states, unlike the one-dimensional Anderson model prediction, is called the "necklace" model [10]. This model has been used in a multilayer dielectric structure [11].

A periodic structure with a transmission spectrum that does not have any propagating modes in certain frequency regions is called the photonic crystal [12]. Frequency spectrum, in which there are no propagating modes, is known as photonic band gap. Due to the vectorial nature of the electromagnetic waves, compared with the scalar nature of electron waves, the emission of electromagnetic waves in photonic crystals depends on its polarization and the wave propagation angle [13].

In a binary multi-layer structure made up of dielectric slabs, in which the optical lengths of the layers are equal, putting the disorder in the order of the layers leads to the appearance of necklace modes in the photonic band gap [14]. By placing a positional disorder in a multilayer structure, when the optical length of layer is equal to a quarter wavelength, a series of transmission modes through the photonic band gap are created [15].

Photonic crystals contain ferroelectric materials, due to the unique properties that compensate for the phase mismatch in the second harmonic generation, which have been much considered. Second harmonic generation is investigated in multilayer nonlinear structures including ferroelectrics such as $LiNbO_3$, $KTiOPO_4$ and strontium barium niobate [16] [17].

But until now, the effect of the disorder on the second harmonic generation (SHG) in the photonic crystals including ferroelectric materials has not been studied. We investigate the effects of positional disorder on the transmission spectrum of one-dimensional structures composed of lithium tantalite ($LiTaO_3$). We study a binary disordered system composed of N periods. Using the transfer matrix method, we draw the transmission spectrum of the electromagnetic wave as a function of the incoming wave frequency. We study the effect of the positional disorder on the transmission of an electromagnetic wave that collides vertically on the surface of the structure, so that during the initial wave propagation

in the nonlinear structure, a second harmonic wave is also produced.

This paper is organized as follows in Section 2 we focus on the details of the model and we derive the related transfer matrix. We also explain how we calculate the Transmission coefficient. In Section 3 we present and discuss our numerical results. Finally, Section 4 ends the paper with a summary of our results.

2. Model and Method

In this section, we study a multi-layered nonlinear structure, which changes the nonlinear parameter sign periodically in layers. In this structure, the scales of linear and nonlinear parameters are the same. The nonlinear structure is divided into N periods of thickness d, and each period is divided into two homogeneous sections, **Figure 1**. Thickness and linear parameter (refractive index) and nonlinear parameter (second order susceptibility) for Section 1 are, respectively, d_I, $n_I^{(r)}$ and $\chi^{(2)}$, while those for Section 2 are, d_{II}, $n_{II}^{(r)}$ and $-\chi^{(2)}$, while $r = f, s$ is use for the fundamental field and second harmonic field, respectively. Due to the fact that the refractive index of regions I ($n_I^{(r)}$) and II ($n_{II}^{(r)}$) are not equal, its reflection will occur at each layer interface, resulting in between the transmitted and reflective waves in each layer, the phenomenon of interference will appear.

It is assumed that an electromagnetic wave with frequency ω incident from the left-hand side of the system and propagates in the direction of the z axis, so that the polarization of the electric field is in the x-axis direction. Our numerical calculations are based on the nonlinear transfer matrix method (TMM) [18] [19]. In this method, the SHG process is divided into three stages: 1) First, the fundamental field (FF), with the propagation in the structure, causes the macroscopic polarization of matter. 2) Since the material is non-linear, then the second-order nonlinear polarization is created in matter. And this nonlinear polarization radiates the second harmonic (SH) field in the structure. 3) This second harmonic field is propagated in the device, and it comes out in the form of a second harmonic signal.

In the first stage of the second harmonic generation, the fundamental and second harmonic fields follow the following equations:

$$\begin{aligned} \nabla\times\left(\nabla\times\boldsymbol{E}_{2\omega}\right)-\frac{\varepsilon_{2\omega}\left(2\omega\right)^2}{c^2}\boldsymbol{E}_{2\omega} &= \mu_0\left(2\omega\right)^2\boldsymbol{P}_{NL}^{2\omega} \\ \nabla\times\left(\nabla\times\boldsymbol{E}_{\omega}\right)-\frac{\varepsilon_{\omega}\omega^2}{c^2}\boldsymbol{E}_{\omega} &= \mu_0\omega^2\boldsymbol{P}_{NL}^{\omega} \end{aligned} \tag{1}$$

In which, ε_{ω}, $\varepsilon_{2\omega}$, $\boldsymbol{P}_{NL}^{\omega}$, and $\boldsymbol{P}_{NL}^{2\omega}$ are permittivity and nonlinear polarization at *FF* and *SH* frequencies. Because the nonlinear process is weak. As a result, the nonlinear process has no significant effect on the intensity of the fundamental pump field (Given that the material we have used in this paper is ferroelectric ($LiTaO_3$), whose second-order non-linear coefficient $\chi^{(2)}$ is 13.8 pm/V. Therefore, in our calculations, we used the source approximation without decreasing (strong source approximation) to solve non-linear equations and

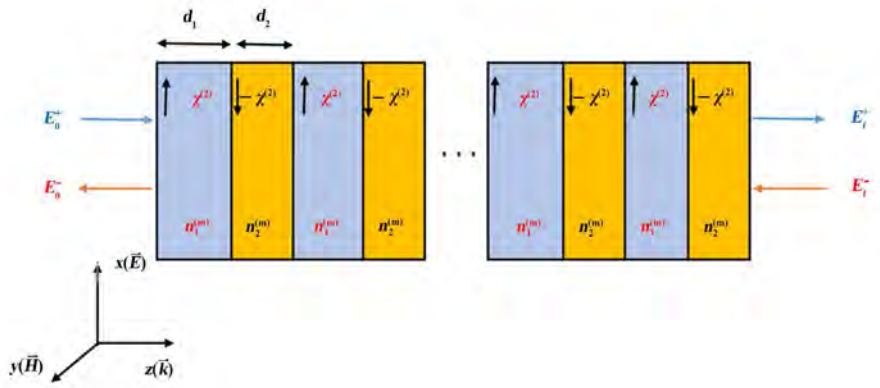

Figure 1. Multi-layered nonlinear structure. In each layer, the vectors represent the nonlinear polarization direction.

obtaining the transmission coefficient. That is, the second-order nonlinear coefficient is small, so the nonlinear process does not have a significant effect on the initial wave intensity). So here we are using the non-depleted pump wave approximation, $E_{2\omega} \ll E_{\omega}$. Therefore, the above equations for the m-th layer are as follows

$$\begin{aligned} &\left[\frac{\mathrm{d}^2}{\mathrm{d}z^2}+\left(k_m^{(f)}\right)^2\right]E_m^f(z)=0 \\ &\left[\frac{\mathrm{d}^2}{\mathrm{d}z^2}+\left(k_m^{(s)}\right)^2\right]E_m^s(z)=-\mu_0(2\omega)^2\boldsymbol{P}_{NL}^{2\omega} \end{aligned} \tag{2}$$

where $k_m^{(f)}=n_m^{(f)}k_0^{(f)}$, $k_m^{(s)}=n_m^{(s)}k_0^{(s)}$, $k_0^{(f)}=\omega/c$, and $k_0^{(s)}=2\omega/c$. and also, $n_m^{(f)}$ and $n_m^{(s)}$ show the refractive index of the pump waves and the second harmonic, respectively in the mth slab; c, the speed of light is in vacuum

The first equation of coupling Equations (2) gives the fundamental electric field in the mth layer.

$$E_m^{(f)}=E_m^{f+}\mathrm{e}^{i\left(k_m^{(f)}(z-z_{m-1})-\omega t\right)}+E_m^{f-}\mathrm{e}^{-i\left(k_m^{(f)}(z-z_{m-1})-\omega t\right)} \tag{3}$$

where z_0 is zero, $z_m=z_{m-1}+d_m$ and d_m is the thickness of the mth layer. $E_m^{(f)+}$ is the magnitude of forward plane wave and $E_m^{(f)-}$ is the magnitude of backward plane wave at the left interface of the mth layer.

According to the continuity conditions on the boundary of the layers, we have the following matrix relation between the electric and magnetic fields passing through odd layer to even layer:

$$\begin{pmatrix} E_{2m-1}^{f+} \\ E_{2m-1}^{f-} \end{pmatrix}=\frac{1}{2n_I^{(1)}}\begin{pmatrix} n_I^{(1)}+n_{II}^{(1)} & n_I^{(1)}-n_{II}^{(1)} \\ n_I^{(1)}-n_{II}^{(1)} & n_I^{(1)}+n_{II}^{(1)} \end{pmatrix}\begin{pmatrix} E_{2m}^{f+} \\ E_{2m}^{f-} \end{pmatrix}=T_{12}\begin{pmatrix} E_{2i}^{f+} \\ E_{2i}^{f-} \end{pmatrix} \tag{4}$$

Using the matrix of dynamics and the matrix of propagation that are as follows.

$$D_m=\begin{pmatrix} 1 & 1 \\ n_m^{(f)} & -n_m^{(f)} \end{pmatrix}$$

$$P_m=\begin{pmatrix} \exp\left(ik_m^{(f)}d_m\right) & 0 \\ 0 & \exp\left(-ik_m^{(f)}d_m\right) \end{pmatrix}$$

The general transfer matrix for the multi-layer structure is as follows

$$T = D_0^{-1}\left(D_{II}P_{II}D_{II}^{-1}D_IP_ID_I^{-1}\right)^N D_0 \tag{5}$$

This transfer matrix connects the fields at the beginning and the end of the structure, as follows

$$\begin{pmatrix} E_t^{f+} \\ E_t^{f-} \end{pmatrix} = T\begin{pmatrix} E_0^{f+} \\ E_0^{f-} \end{pmatrix} \tag{6}$$

For harmonic fields that is produced in the structure, we use Equation (2) with $P_{NL}^{2\omega}(z,t) = \varepsilon_0\chi_m^{(2)}\left[E_m^{(f)}(z)\right]^2\exp(-i2\omega t)$ that yields to:

$$\begin{aligned}\begin{pmatrix} E_m^{(s)+} \\ E_m^{(s)-} \end{pmatrix} &= G_0^{-1}SG_0\begin{pmatrix} E_{m-1}^{(s)+} \\ E_{m-1}^{(s)-} \end{pmatrix} + G_0^{-1}\left(N_{II}B_IF_I - SB_I\right)A_I\begin{pmatrix} \left(E_{2m-1}^{f+}\right)^2 \\ \left(E_{2m-1}^{f-}\right)^2 \end{pmatrix} \\ &+ G_0^{-1}\left(N_{II}-S\right)\begin{pmatrix} C_IE_{2m-1}^{f+}E_{2m-1}^{f-} \\ 0 \end{pmatrix} \\ &+ G_0^{-1}\left(B_{II}F_{II} - N_{II}B_{II}\right)A_{II}\begin{pmatrix} \left(\Omega_{2m}^{+}\right)^2 \\ \left(\Omega_{2m}^{-}\right)^2 \end{pmatrix} \\ &+ G_0^{-1}\left(I - N_{II}\right)\begin{pmatrix} C_{II}E_{2m}^{f+}E_{2m}^{f-} \\ 0 \end{pmatrix}\end{aligned} \tag{7}$$

In which:

$$A_l = \frac{-4\mu\varepsilon_0\chi_l^{(2)}\omega^2}{k_l^{(s)2} - 4k_l^{(f)2}}, C_l = \frac{-4\mu\varepsilon_0\chi_l^{(2)}\omega^2}{k_l^{(s)2}}$$

$$G_l = \begin{pmatrix} 1 & 1 \\ n_l^{(s)} & -n_l^{(s)} \end{pmatrix}, B_l = \begin{pmatrix} 1 & 1 \\ \dfrac{2k_0^{(f)}n_l^{(f)}}{k_0^{(s)}} & -\dfrac{2k_0^{(f)}n_l^{(f)}}{k_0^{(s)}} \end{pmatrix}$$

$$Q_i = \begin{pmatrix} \exp\left(ik_l^{(s)}d_i\right) & 0 \\ 0 & \exp\left(-ik_l^{(s)}d_l\right) \end{pmatrix}$$

$$F_l = \begin{pmatrix} \exp\left(i2k_l^{(f)}d_l\right) & 0 \\ 0 & \exp\left(-i2k_l^{(f)}d_l\right) \end{pmatrix} \quad l = I, II$$

$$S = G_{II}Q_{II}G_{II}^{-1}G_IQ_IG_I^{-1}, N_{II} = G_{II}Q_{II}G_{II}^{-1}$$

In this section, we determined the method of obtaining the amplitude of the second harmonic field in the nonlinear multi-layer structure. We can not actually measure this quantity, but the intensity of the second harmonic is measurable (In this paper, which is a theoretical work, the intensity of the waves is obtained using the electromagnetic magnitude (intensity is proportional to the square of the field magnitude). The purpose of writing the phrase "measurable intensity of electromagnetic waves" is that in the laboratory, researchers measure the intensity of electromagnetic waves. In fact, this sentence is presented for

comparison with laboratory work). Using the intensity of waves, we have the following definitions for the nonlinear reflectance and nonlinear transmittance:

$$R^{NL} = \frac{I_{harm}^{r}}{\left(I_{pump}\right)^{2}}$$
$$T^{NL} = \frac{I_{harm}^{t}}{\left(I_{pump}\right)^{2}} \tag{8}$$

where $I_{harm}^{t,r}$ and I_{pump} are the intensities of the reflected or transmitted harmonic and pump fields, respectively.

In our structure, it is assumed that the nonlinear photonic crystal are composed of periodically poled lithium tantalite ($LiTaO_3$) crystal, whose nonlinear susceptibility is $\chi^{(2)} = 13.8\ \text{pm/V}$ and The refractive index for lithium tantalite ($LiTaO_3$) is given by the following dispersion formula [20]:

$$n^2(\lambda, T) = A + \frac{B + b(T)}{\lambda^2 - \left[C + c(T)\right]^2} + \frac{E}{\lambda^2 - F^2} + D\lambda^2 \tag{9}$$

where $A = 4.5284$, $B = 7.2449 \times 10^{-3}$, $C = 0.2453$, $D = -2.3670 \times 10^{-2}$, $E = 7.7690 \times 10^{-2}$, $F = 0.1838$, $b(T) = 2.6794 \times 10^{-8}\left(T + 273.15\right)^2$, $c(T) = 1.6234 \times 10^{-8}\left(T + 273.15\right)^2$.

Periodic polar ferroelectric ($LiTaO_3$) crystals are described by modulations of the nonlinear susceptibilities. An optoelectronic effect is used to produce the photonic band gap structure. This effect is the origin of the modulation of the refractive index of the layers in the photonic crystal. If the electric field E is applied in the direction of the optical axis of the material, correction of refractive index and new refractive index (in odd layers) are as follows:

$$n_1 = n + \Delta n_1 = n - \frac{1}{2} n^3 r_{33} E \tag{10}$$

where r_{33} is the optoelectronic coefficient of the material and E is the electric field amplitude. Similar to the nonlinear optical coefficient, the optoelectronic coefficient of the material in different layers has different signs. So in reverse (even) layers the optoelectronic coefficient changes sign and the refractive index in these layers is written as follows:

$$n_2 = n + \Delta n_2 = n + \frac{1}{2} n^3 r_{33} E \tag{11}$$

3. Numerical Results

We investigate a random binary structure constructed of N lithium tantalite ($LiTaO_3$) layers. The positional disorder in the structure means the probability that the ith layer is Layer I or Layer II is equal. In order to have an overall picture of the role played by disorder, and to illustrate the effect of disorder in the nonlinear multi-layered structure, we compare the transmission spectrum of a periodic structure with alternating layers I and II with a disordered structure, as shown in **Figure 2** for the structure with $N = 70$ layers.

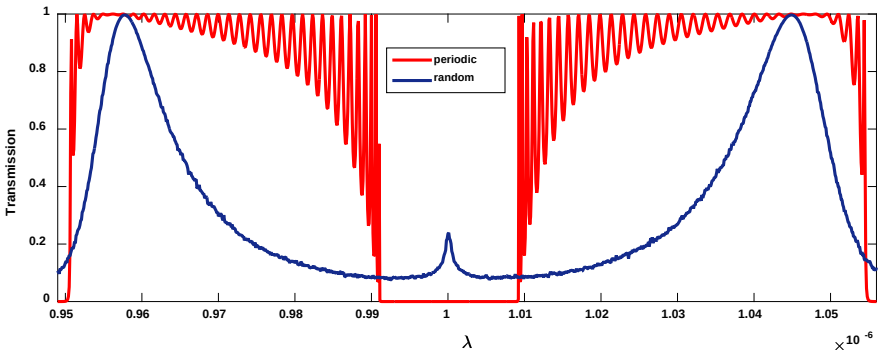

Figure 2. Transmission spectrum of periodic (red) and random (blue) binary structure with N = 70 layers. For the random system, to calculate the transmission coefficient quantity, averaging operations are performed on 3000 systems with different ordering. The placement of disorder has different effects on the transmitting and gap bands. The disorder results in the appearance of transmission modes in the middle of the gap band.

The transmission spectrum for periodic structures is a sequence of transmitting and stop bands. In the transmitting band, there is a frequency in which the optical length of each layer is an integer multiple of half the wavelength in the vacuum. In other words, the phase change in each layer is equal to $m\pi$, that m is the member of the integers. The nonlinear multi-layer structure for this incoming wave frequency is completely transparent. In the center of the stop bands, there are frequencies in which the optical length of each layer is odd multiples of one quarter wavelength. As a result, the phase change in these layers is equal to $(m+1/2)\pi$. For the random system, to calculate the Transmission coefficient quantity, averaging operations are performed on 3000 systems with different ordering (**Figure 2**). The placement of disorder has different effects on the transmitting and gap bands. Firstly, the disorder does not affect the frequency in the transmitting band in which the optical length of each layer is an integer multiple of half the wavelength. In other words, in a periodic and random structure at this frequency, the transmission coefficient is equal to the unit. Note that at this frequency, for each layer, the transfer matrix is a unit matrix (I). In this mode, independent of the existence and absence of disorder in the structure, is similar to the violation of Anderson localization in the random-dimer model. But, by placing disorder in the structure, the width of the transmission band is reduced. In the forbidden (gap) band, the disorder leads to the emergence of a series of transmitting modes. These mods are known as necklace modes.

In order to see the different effects of positional disorder in the transmitting band and the forbidden band, we plot the average transmission coefficient around the half- and quarter-wavelength modes as a function of the disorder intensity. In **Figure 3** and **Figure 4**, q shows the disorder strength, in other words, q is equal to the probability that in the periodic structure (I, II, I, II, I, II, ···, I, II), the ith layer, replaced with another layer. So $q=0$ is related to the periodic structure and $q=1/2$ is a structure with complete disorder. The results are shown in **Figure 3** and **Figure 4** for $N=70$. In order to obtain the transmission

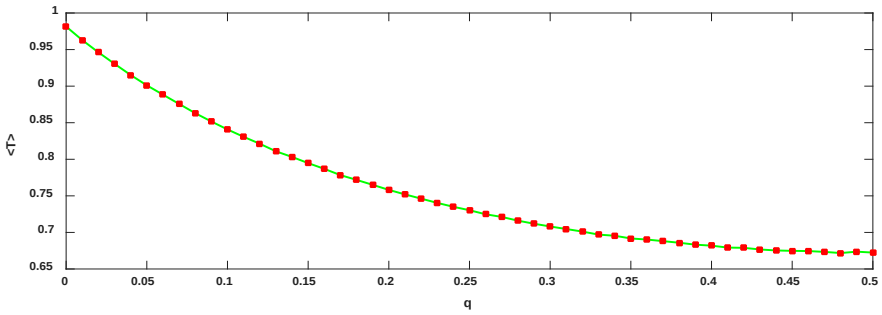

Figure 3. The average transmission coefficient as a function of the severity of the disorder, for the transmitting band. In this case, when the disorder increases, the transmission coefficient decreases, so Anderson's localization is established. The averaging is performed on 3000 structures in different order and $N = 70$.

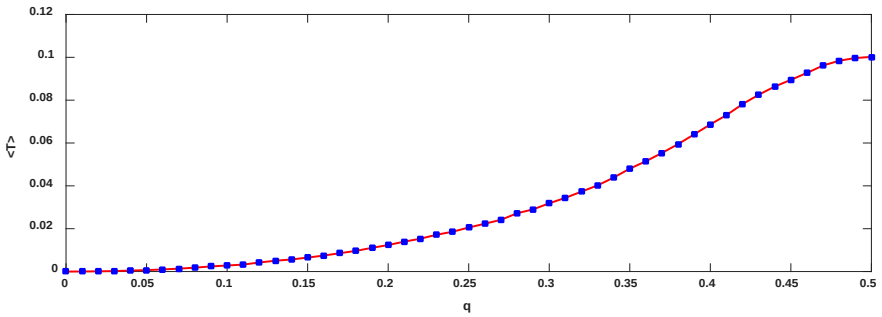

Figure 4. The average transmission coefficient as a function of the severity of the disorder, for the forbidden (gap) band. In quarter-wavelength modes, with increasing disorder, a series of transmitting modes are created, and thus a weak transmittance occurs at these frequencies. The averaging is performed on 3000 structures in different order and $N = 70$.

coefficient in random structures, the averaging is performed on 3000 structures in different order. **Figure 3** for the transmitting band and **Figure 4** for forbidden band.

For the average transmission coefficient around the half-wavelength resonance, when the disorder increases, the transmission coefficient decreases, so Anderson's localization is established (**Figure 3**). Meanwhile, disorder effect in an around the quarter-wavelength resonance mode have a completely reverse result. As the disorder increases, the average transmittance increases (**Figure 4**). The reason for this is the appearance of transmitting modes in the forbidden band (Because in the periodic structure, in the gap band, the interference of the waves is non constructive. Using a disorder in the arrangement of the layers, the periodic structure that causes non-constructive interference of the waves and the transmission coefficient 0 in this frequency region (gaps) collapses. And with increasing disorder, the effect of the structure on the non-constructive interference of the waves decreases. As a result, the waves interact constructively. And there is a series of poorly transmitted modes in the gap band).

Figure 3 shows the average transmission coefficient in the transmitting band according to Anderson's localization. In this case, the average transmittance coefficient decreases monotonically with increasing intensity disorder.

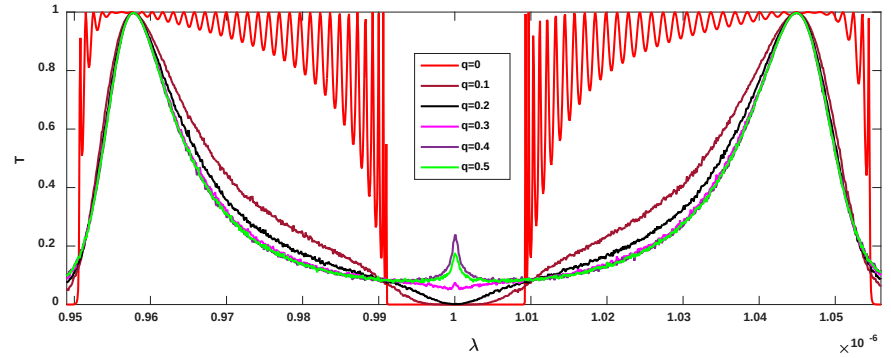

(a)

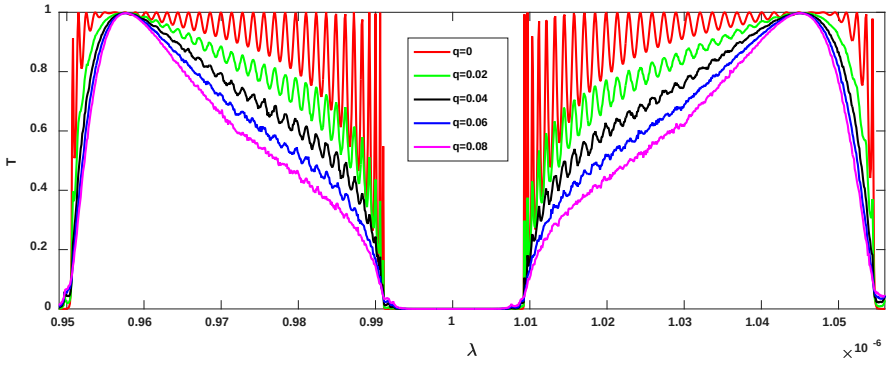

(b)

Figure 5. Transmission coefficient for different values of the disorder intensity. The number of layers is 70 and the averaging is performed on 2500 structures in different order. **Figure 5(a)** shows strong intensity disorder, in which case Anderson's theory is violated in the band gap. **Figure 5(b)** is for weak intensity disorders, in which case Anderson's localization is established.

While **Figure 4** is a violation of Anderson's theory, the disorder result in the emergence of a few resonance necklace modes that creates a small transmittance in gap band.

Figure 5 shows the transmission coefficient as a function of the collision wavelength for different degrees of disorder. By increasing Severity of disorder, the bandwidth of transmission is reduced and a series of necklace mode is created in the gap bands which cause a slight increase in the transmission coefficient of electromagnetic waves. **Figure 5(b)** is for weak intensity disorders, in which case Anderson's localization is established. **Figure 5(a)** shows strong intensity disorder, in which case Anderson's theory is violated in the band gap.

4. Results

We studied the transmittance spectra in a nonlinear structure composed of tantalum lithium ($LiTaO_3$). This system is a binary structure with N layer. The effect of disorder on the transmitting and forbidden bands is quite distinct. For the transmission band, the disorder in the frequency at which the coefficient of transmission is equal to 1 does not affect. At this frequency, the transfer matrix of each layer is equal to the unit matrix (I). The lack of sensitivity of this fully

resonance mode is similar to the violation of Anderson's theory in the random-dimer model. However, the width of the transmittance band in a disordered system is narrower than the width of the transmittance band of the periodic system. For the gap band, disorder lead to the appearance of several modes in the center of the band. These modes are called necklace modes, which are based on the hybridization of degenerate modes localized. The transmittance in the stop (gap) band increases with the disorder intensity. The transmittance in the transmitting band decreases with the disorder intensity.

Conflicts of Interest

The authors declare no conflicts of interest regarding the publication of this paper.

References

[1] Anderson, P.W. (1958) *Physical Review*, **109**, Article ID: 1492. https://doi.org/10.1103/PhysRev.109.1492

[2] Abrahams, E., Anderson, P.W., Licciardello, D.C. and Ramakrishnan, T.V. (1979) *Physical Review Letters*, **42**, Article ID: 673. https://doi.org/10.1103/PhysRevLett.42.673

[3] Kramer, B. and MacKinnon, A. (1993) *Reports on Progress in Physics*, **56**, 1469. https://doi.org/10.1088/0034-4885/56/12/001

[4] Dunlap, D.H., Wu, H.-L. and Phillips, P.W. (1990) *Physical Review Letters*, **65**, Article ID: 88. https://doi.org/10.1103/PhysRevLett.65.88

[5] Phillips, P.W. and Wu, H.L. (1991) *Science*, **252**, 1805-1812. https://doi.org/10.1126/science.252.5014.1805

[6] de Moura, F.A.B.F. and Lyra, M.L. (1998) *Physical Review Letters*, **81**, Article ID: 3735.

[7] Domínguez-Adame, F., Malyshev, V.A., de Moura, F.A.B.F. and Lyra, M.L. (2003) *Physical Review Letters*, **91**, Article ID: 197402. https://doi.org/10.1103/PhysRevLett.91.197402

[8] Theodorou, G. and Cohen, M. (1976) *Physical Review B*, **13**, Article ID: 4597. https://doi.org/10.1103/PhysRevB.13.4597

[9] Fleishman, L. and Licciardello, D.C. (1977*) Journal of Physics C*, **10**, L125.

[10] Pendry, J.B. (1994) *Advances in Physics*, **43**, 461-542. https://doi.org/10.1080/00018739400101515

[11] Bertolotti, J., Gottardo, S., Wiersma, D.S., Ghulinyan, M. and Pavesi, L. (2005) *Physical Review Letters*, **94**, Article ID: 113903. https://doi.org/10.1103/PhysRevLett.94.113903

[12] Yablonovitch, E. (1987) *Physical Review Letters*, **58**, Article ID: 2059. https://doi.org/10.1103/PhysRevLett.58.2059

[13] Fan, S.H., Villeneuve, P.R. and Joannopoulos, J.D. (1996) *Physical Review B*, **54**, Article ID: 11245. https://doi.org/10.1103/PhysRevB.54.11245

[14] Sebbah, P., Hu, B., Klosner, J.M. and Genack, A.Z. (2006) *Physical Review Letters*, **96**, Article ID: 183902. https://doi.org/10.1103/PhysRevLett.96.183902

[15] Bertolotti, J., Galli, M., Sapienza, R., Ghulinyan, M., Gottardo, S., Andreani, L.C., Pavesi, L. and Wiersma, D.S. (2006) *Physical Review E*, **74**, Article ID: 035602.

[16] Piskarskas, A., Smilgevicius, V., Stabinis, A., Jarutis, V., Pasiskevicius, V., Wang, S., Tellefsen, J. and Laurell, F. (1999) *Optics Letters*, **24**, 1053-1055. https://doi.org/10.1364/OL.24.001053

[17] Zhu, Y.Y., Fu, J.S., Xiao, R.F. and Wong, G.K. (1997) *Applied Physics Letters*, **70**, 1793-1795. https://doi.org/10.1063/1.118694

[18] Bell, P.M., Pendry, J.B., Marin Moreno, L. and Ward, A.J. (1995) *Computer Physics Communications*, **85**, 306-322. https://doi.org/10.1016/0010-4655(94)00131-K

[19] Lin, L.L., Li, Z.Y. and Ho, K.M. (2003) *Journal of Applied Physics*, **94**, 811-821. https://doi.org/10.1063/1.1587011

[20] Meyn, J.P. and Fejer, M.M. (1997) *Optics Letters*, **22**, 1214-1216. https://doi.org/10.1364/OL.22.001214

Journal of Modern Physics, 2019, 10, 443-451
http://www.scirp.org/journal/jmp
ISSN Online: 2153-120X
ISSN Print: 2153-1196

Determination of Fourier Components of Spatial Correlation Function of Dielectric Susceptibility of Random Medium

Ning Mu, Wanrong Gao

Department of Optical Engineering, Nanjing University of Science and Technology, Nanjing, China
Email: wgao@njust.edu.cn

How to cite this paper: Mu, N. and Gao, W. (2019) Determination of Fourier Components of Spatial Correlation Function of Dielectric Susceptibility of Random Medium. *Journal of Modern Physics*, **10**, 443-451.
https://doi.org/10.4236/jmp.2019.104029

Received: February 8, 2019
Accepted: March 16, 2019
Published: March 19, 2019

Abstract

In this work, we present a new method of directly determining Fourier components of the spatial correlation function of the dielectric susceptibility of random medium. The method is based on the analysis of the ratio of the spectrum of the light scattered by the spatial correlation components of the dielectric susceptibility of tissue to the spectrum of light scattered by the randomly distributed scatterers which are independent on the value of the spectrum of the incident light and the direction of the observation. The results may find wide applications in areas such as in biomedical diagnosis.

Keywords

Spatial Correlation of Refractive Index, Spectrum of the Light Scattered, Dielectric Susceptibility, Fourier Components

1. Introduction

When light propagates through a random medium such tissue, it will be scattered due to the spatial variations of the refractive index of the tissue. The properties of the scattered light are dependent on both the properties of the incident light and the three-dimensional (3D) microstructures of the tissue. The relationships that exist between the properties of the scattered light and properties of the structure of the object under investigation can be explored to obtain information about cells and tissues.

In 1989, Wolf *et al.* investigated the scattering of polychromatic light by a medium whose dielectric susceptibility is a random function of position [1]. However, their concern is on the frequency shifts of the spectral density due to the

scattering process. They found that the spectrum of the scattered light is dependent on both the spectrum of the incident light and the Fourier components of the spatial correlation function of the dielectric susceptibility of the random medium. For light propagating through random medium, changes in coherence, polarization and spectrum of light have also been considered [2]-[12]. These results may be explored to derive some information about structures of tissues [13] [14] [15] [16].

Information about cell and tissue structures can also be obtained by combing measured properties of reflected and scattered light with theoretical models. In fact, it has been shown that the size distribution of the cell nuclei can be obtained by fitting measured light scattering spectra to the predictions of Mie theory [17]. In addition, by analyzing the amplitude and frequency of a fine structure component in backscattered light, the density and size distribution of epithelial cell nuclei can be extracted [18] [19]. Finally, it was also found that some Fourier components of the spatial correlation functions of refractive index fluctuations of living tissues can be measured by Fourier domain optical coherence tomography (FDOCT) [8] [13] [20].

Tissue has very complex structures and can be decomposed into different components from different points of view. It can be approximately represented by a structure consisting of an infinite number of particles with sizes within a large range in which the refractive index variations can be approximately generated by spherical particles with some size distribution (for example) [21]. The particle model of light scattering in tissue is appropriate in cases where the imaging resolution is much larger than the size of the scatterers [22]. At the microscopic level, there is no clear interface between constituents of tissue. A continuous model of refractive index was then proposed in which refractive index variation is represented by a continuous function of position within tissue [23]-[28].

It has been demonstrated experimentally that at the microscopic level, there is a degree of spatial correlation among tissue structures between any two points [2]-[28]. In this work, we present a new method of directly determining Fourier components of the spatial correlation function of the dielectric susceptibility of random medium. First, the ratio is derived of the spectrum of the light scattered by the spatial correlation components of the dielectric susceptibility of tissue to the spectrum of light scattered by the randomly distributed scatterers. It is found that the ratio of the spectrum of the scattered light induced by the spatial correlation of the refractive index fluctuations to the spectrum of the scattered light generated by the randomly distributed scatterers is independent on the value of the incident spectrum. There is also no ω^4 factor in the ratio. A new method is proposed for directly determining Fourier components of the spatial correlation function of the dielectric susceptibility of random medium. A model for characterizing the Fourier spectrum of the refractive index correlation function of tissue is used as an example to demonstrate the analysis. The results obtained may find wide applications in areas such as in biomedical diagnosis.

2. Theory

Within the accuracy of the first-order born approximation, the spectrum $S^{(\infty)}(r\boldsymbol{s},\omega)$ of the light scattered by deterministic medium and observed in the far zone can be expressed as Equation (1)

$$S^{(\infty)}(r\boldsymbol{s},\omega)=\frac{1}{r^2}\left(\frac{\omega}{c}\right)^4\tilde{\eta}^*\left[k(\boldsymbol{s}-\boldsymbol{s}_0),\omega\right]\tilde{\eta}\left[k(\boldsymbol{s}-\boldsymbol{s}_0),\omega\right]S^{(i)}(\omega), \tag{1}$$

where * denotes the complex conjugate, $k=\omega/c=2\pi/\lambda$ is the wavenumber, ω is the frequency of the light, c is the speed of light in vacuo, λ is the wavelength, $\boldsymbol{s}$ is the unit vector in the direction of scattering, r is the distance from the observation point to the reference point, $\boldsymbol{s}_0$ is a real unit vector in a direction, $S^{(i)}(\omega)$ is the spectrum of the incident light, and

$$\tilde{\eta}\left[k(\boldsymbol{s}-\boldsymbol{s}_0),\omega\right]=\int_{V(\boldsymbol{r}')}\eta(\boldsymbol{r}',\omega)\exp\left[-jk(\boldsymbol{s}-\boldsymbol{s}_0)\cdot\boldsymbol{r}'\right]\mathrm{d}^3r', \tag{2}$$

is the Fourier transform of the dielectric susceptibility $\eta(\boldsymbol{r},\omega)=\left[n^2(\boldsymbol{r},\omega)-1\right]/4\pi$, $n(\boldsymbol{r},\omega)$ is the refractive index of the medium (see Figure 1). Equation (1) is valid when the amplitude of the scattered light field is small compared with the amplitude of the incident field. It can be seen from Equation (1) that in this case, by measuring the spectrum of the scattered light, one can directly obtain the Fourier components represented by the spatial frequency vector $\boldsymbol{K}=k(\boldsymbol{s}-\boldsymbol{s}_0)$ in $\boldsymbol{K}$ space. The Fourier components available, of course, are determined by the range of the wavenumber of the incident light and the directions of the observation achievable.

Note that the basic principle of the Fourier domain optical coherence tomography (FDOCT) is based on the interferometric measurement of one dimension simplified version of Equation (1) [29] [30] [31] [32] [33].

For the random scattering medium, its refractive index and dielectric susceptibility fluctuate with position, which causes scattering of light. An ensemble average is then needed to find the expectation value of the spectrum in Equation (1). We have [1]

$$S_c^{(\infty)}(r\boldsymbol{s},\omega)=\frac{1}{r^2}\left(\frac{\omega}{c}\right)^4\tilde{C}_\eta\left[-\boldsymbol{K},\boldsymbol{K},\omega\right]S^{(i)}(\omega), \tag{3}$$

where $\tilde{C}_\eta$ is the Fourier transform of the spatial correlation function $C_\eta(\boldsymbol{r}_1',\boldsymbol{r}_2',\omega)=\left\langle\eta^*(\boldsymbol{r}_1',\omega)\eta(\boldsymbol{r}_2',\omega)\right\rangle$ of the dielectric susceptibility and is defined as

$$\begin{aligned}\tilde{C}_\eta(\boldsymbol{K}_1,\boldsymbol{K}_2,\omega)a&=\left\langle\tilde{\eta}(\boldsymbol{K}_1,\omega)\tilde{\eta}^*(\boldsymbol{K}_2,\omega)\right\rangle\\&=\int_V\int_V C_\eta(r_1',r_2',\omega)\exp\left[-j(\boldsymbol{K}_2\cdot\boldsymbol{r}_2'-\boldsymbol{K}_1\cdot\boldsymbol{r}_1')\right]\mathrm{d}^3\boldsymbol{r}_1'\mathrm{d}^3\boldsymbol{r}_2'\end{aligned} \tag{4}$$

Equation (3) shows that, for the random scattering medium, the spectrum of the scattered light observed in the direction $\boldsymbol{s}$ in the far zone is proportional to the product of a factor proportional to ω^4 and the Fourier component of the spatial correlation function of the dielectric susceptibility with the spatial frequency vector $\boldsymbol{K}=k(\boldsymbol{s}-\boldsymbol{s}_0)$ in $\boldsymbol{K}$ space. On the other hand, Equation (1)

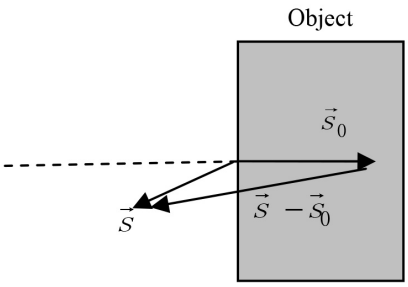

Figure 1. Illustrating the notations. The real unit vector $\boldsymbol{s}_0$ denotes the direction of the incident light, the real unit vector $\boldsymbol{s}$ denotes the direction of the scattered light, and $\boldsymbol{K}=k(\boldsymbol{s}-\boldsymbol{s}_0)$ is the spatial frequency vector.

reveals that for deterministic medium, the spectrum observed in the direction $\boldsymbol{s}$ is proportional to the square of the Fourier component of the dielectric susceptibility itself.

Thus when there exist spatial correlated fluctuations in the dielectric susceptibility or refractive index of the medium, the Fourier component of the dielectric susceptibility is also random function. In this case, it is the spatial correlation of the dielectric susceptibility that determines the spectrum of the scattered light.

In the case when the dielectric susceptibility of the medium is completely uncorrelated, we have

$$\begin{aligned} C_\eta(\boldsymbol{r}_1',\boldsymbol{r}_2',\omega) &= I(\omega)\delta^{(3)}(\boldsymbol{r}_2'-\boldsymbol{r}_1') \quad \text{when} \quad \boldsymbol{r}_1'\in V,\ \boldsymbol{r}_2'\in V \\ &= 0 \qquad\qquad\qquad\qquad\quad \text{otherwise,} \end{aligned} \tag{5}$$

where $\delta^{(3)}(\boldsymbol{r}')$ is the 3D Dirac delta function and $I(\omega)$ is a nonnegative function of frequency. In this case, from Equation (3) we have:

$$S_u^{(\infty)}(r\boldsymbol{s},\omega)=\frac{1}{r^2}\left(\frac{\omega}{c}\right)^4 I(\omega)S^{(i)}(\omega). \tag{6}$$

We can see from Equation (6) that for a given frequency ω of light, there is no observation direction dependence of the spectrum of the scattered light. Note that when the dielectric susceptibility of the medium is completely uncorrelated, from the measured spectrum of the scattered light, we can obtain no information about the spatial correlated structure of the scatterers, as expected. This fact has important implications in the biomedical imaging of tissues. For example, this fact shows that it is then possible to detect some forms of variations of tissue structures by analyzing properties of ratio of the spectrum of the light scattered by the spatial correlation of the fluctuations of the tissue refractive index and the scattered light arising from the deterministic change of the refractive index such as in the small interfaces between different tissue elements.

For the light scattering induced by the spatial correlation of the refractive index fluctuations, there is an intimate relationship between its spectrum and the Fourier components of the of the spatial correlation function of the dielectric susceptibility. Notice that it has been found experimentally that there exists only

finite spatial correlation length between the fluctuations of tissue refractive index at two points. For tissues, the spatial correlation length is found to equal or exceed 4 μm [16]. Thus, tissue elements with sizes larger than the spatial correlation may be regarded as being randomly distributed. In this case, there is no scattering due to the correlation of its refractive index.

If we calculate the ratio of Equation (3) to Equation (6) and denote it by $R_S^{(\infty)}$, we have

$$R_S^{(\infty)}(r\boldsymbol{s},\omega)=\frac{S_c^{(\infty)}(r\boldsymbol{s},\omega)}{S_u^{(\infty)}(r\boldsymbol{s},\omega)}=\frac{\tilde{C}_\eta[-\boldsymbol{K},\boldsymbol{K},\omega]}{I(\omega)}. \tag{7}$$

Equation (7) demonstrates that the ration $R_S^{(\infty)}$ is equal to the ratio of the Fourier component of the spatial correlation function of the dielectric susceptibility to a function of the frequency. From Equation (7) we can see that the ratio of the spectrum of the scattered light induced by the spatial correlation of the refractive index fluctuations to the spectrum of the scattered light generated by the randomly distributed scatterers is independent on the value of the incident spectrum. There is also no ω^4 factor in the ratio. Thus, the value of the ratio may reveal some inherent micro-structural characteristics of the scattering medium.

3. Method

Now we consider a specific case when incident light is monochromatic or with a very small bandwidth. In this case, $I(\omega)$ can be regarded as a constant $I(\omega_0)$, where ω_0 the average frequency of the light. For different observation direction, denoted by $\boldsymbol{s}$, $R_S^{(\infty)}$ is equal to the ratio of the Fourier component of the spatial correlation function of the dielectric susceptibility with the spatial frequency vector $\boldsymbol{K}=k(\boldsymbol{s}-\boldsymbol{s}_0)$ to the constant $I(\omega_0)$. In this case, we have

$$\tilde{C}_\eta[-\boldsymbol{K},\boldsymbol{K},\omega_0]=R_S^{(\infty)}(r\boldsymbol{s},\omega_0)I(\omega_0). \tag{8}$$

Equation (8) shows that if we have the knowledge about $I(\omega_0)$, for a given value of ω_0, we can directly obtain the values of $\tilde{C}_\eta[-\boldsymbol{K},\boldsymbol{K},\omega_0]$.

The spatial correlation function of the dielectric susceptibility is an important parameter for characterizing the effects of the random medium on the propagation properties of light within it. It is related to the refractive index correlation function. Consider the case of tissue, if we express refractive $n(\boldsymbol{r},\omega)$ index in the form of $n(\boldsymbol{r},\omega)=\langle n(\boldsymbol{r},\omega)\rangle+\delta n(\boldsymbol{r},\omega)$, where $\boldsymbol{r}$ denotes the position within the medium, $\langle n(\boldsymbol{r},\omega)\rangle$ is the mean of the refractive index, $\delta n(\boldsymbol{r},\omega)$ is the varying part of refractive index with position, it has been shown that [4]

$$C_\eta(\boldsymbol{r}_1,\boldsymbol{r}_2,\omega)=(1/16\pi^2)\left(\langle n\rangle^4-2\langle n\rangle^2+1+4\langle n\rangle^2 C_n(\boldsymbol{r}_1,\boldsymbol{r}_2,\omega)\right), \tag{9}$$

where $C_n(\boldsymbol{r}_1,\boldsymbol{r}_2,\omega)=\langle\delta n(\boldsymbol{r},\omega_1)\delta n(\boldsymbol{r}_2,\omega)\rangle$ is the refractive index correlation function. The Fourier transform of the spatial correlation function of the dielectric susceptibility can then be expressed as

$$\tilde{C}_{\eta}(K,\omega)=\left[1/(4\pi)^2\right]\langle n\rangle^2\,\Phi(K), \tag{10}$$

where $\Phi(K)$ is the Fourier spectrum of the refractive index correlation function of tissue. For tissue samples, $\Phi(K)$ has been measured and is of the form [23]

$$\Phi(K)=4\pi\sigma_n^2L_0^2(m-1)\left(1+K^2L_0^2\right)^{-m}, \tag{11}$$

where L_0 is the outer scale of tissue index inhomogeneities, $L_0=l_c/\left[2(m-1)^{1/2}\right]$, m is a parameter (1 < m < 2), where σ_n is the standard deviation of the refractive index, l_c is the index correlation distance, and

$$K=|\boldsymbol{K}|=|\boldsymbol{k}-\boldsymbol{k}_0|=2k\sin(\theta/2), \tag{12}$$

where θ is the angle between the unit vector $\boldsymbol{s}_0$ along the incident direction and the unit vector $\boldsymbol{s}$ along the observation direction, respectively. **Figure 2** shows the normalized curve of the variation of the ration $R_S^{(\infty)}$ with the observation direction for the light backscattered from the human upper dermis [23].

The refractive index correlation function determines the light scattering characteristics in tissue as well as the changes of the coherence and polarization of the light beam propagating through tissue [2]-[8]. Equation (10) shows that the Fourier spectrum of the refractive index correlation function of tissue may be obtained by measuring the spectrum of the scattered light through relations (8) and (10). Here, it should be emphasize that the result obtained in this work is based on the first-order born approximation. In our analysis, it is also assumed that the scattering properties of the medium can be described by its refractive index $n(\boldsymbol{r},\omega)$ which is a three-dimensional function of position $\boldsymbol{r}$.

A comparison of Equation (5) with Equation (9) shows that when dispersion effect of the tissue can be neglected, we have:

$$I(\omega_0)=\frac{\langle n(\omega_0)\rangle^2}{4\pi^2}. \tag{12}$$

Equation (12) demonstrates that the value of $I(\omega_0)$ can be obtained by measuring the mean of the refractive index and using the Equation (12). One possible method for measuring the ration $R_S^{(\infty)}$ is to use the fact that the spectrum of the light scattered by the spatially correlated structures of the dielectric susceptibility is a function of the angle of scattering and there is no observation direction dependence of the spectrum of the light scattered by completely uncorrelated components. So the angle varying part of the measured spectrum of the scattered light represents the contribution of the spatially correlated structures of the dielectric susceptibility and the angle independent part describes the contribution due to the completely uncorrelated components of the medium.

In general, the real medium, such as living tissue, is a complex system, in which light is scattered or reflected by various aspects of its structure. First of all, the layer structures of tissue may be regarded as its deterministic aspect. In this case, the spectrum of the scattered light is related to the Fourier transform of the

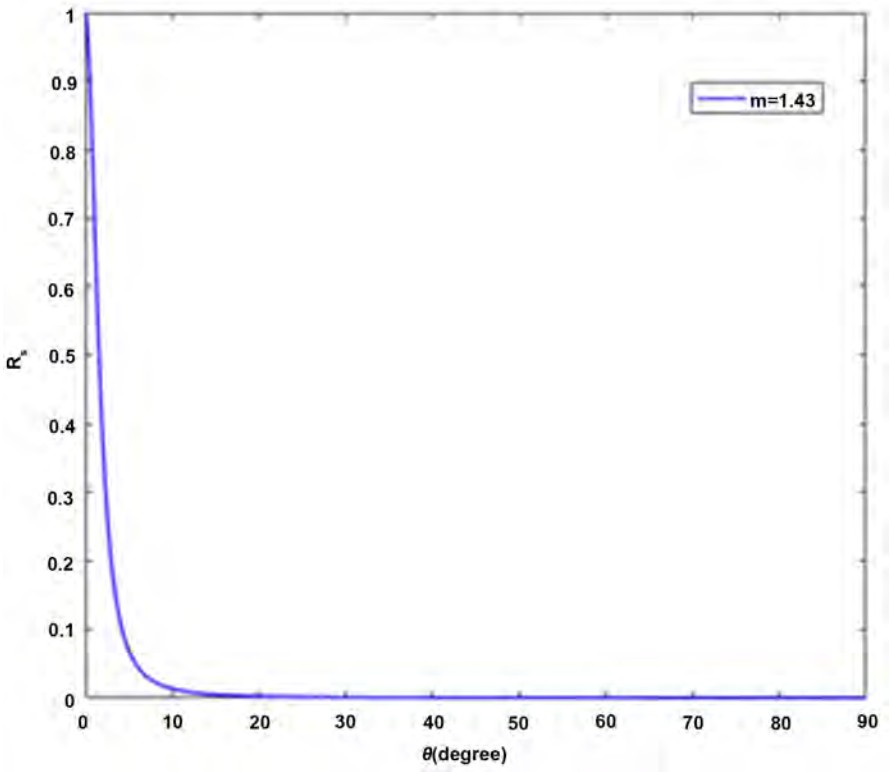

Figure 2. The normalizd curve of variation of the ration $R_S^{(\infty)}$ with the observation direction for some selected values of the parameters. $\langle n \rangle$ = 1.35, σ_n = 0.06, m = 1.43, L_0 = 4 μm, λ_c = 0.83 μm.

dielectric susceptibility, as is also shown in the images obtained with FDOCT [14]. Second, for the microscopic structures that have no clear layer structure, the scattering of light may arise from the spatial fluctuations of the refractive index and the spectrum of the scattered light is related to the Fourier component of the spatial correlation function of the dielectric susceptibility, which reveals the microscopic morphological information about the cells or tissues.

In conclusion, we have demonstrated that the ratio of the spectrum of the scattered light induced by the spatial correlation of the dielectric susceptibility to the spectrum of the scattered light generated by the randomly distributed scatterers is independent on the value of the incident spectrum. There is also no ω^4 factor in the ratio. The results supply us a new method for direct determination of Fourier components of the spatial correlation function of the dielectric susceptibility of random medium by measuring the spectrum of the scattered light field, including atmospheric turbulence, oceanic turbulence, and biological tissue. Because the spatial correlation characteristics of the dielectric susceptibility of random medium is a manifestation of the underlying process that produces local correlations in the positions of growing cells in living tissue, the work has potential application in biomedical diagnosis.

Define abbreviations and acronyms the first time they are used in the text, even after they have been defined in the abstract. Abbreviations such as IEEE, SI,

MKS, CGS, sc, dc, and rms do not have to be defined. Do not use abbreviations in the title or heads unless they are unavoidable.

Acknowledgements

This work was supported by the Natural Science Foundation of China (NSFC) (61275198, 60978069) and the Key special Projects of "Major Scientific Instruments and Equipment Development" of the National Key Research and Development Plan, Ministry of Science and Technology, P. R. China (2017YFF0107100).

Conflicts of Interest

The authors declare no conflicts of interest regarding the publication of this paper.

References

[1] Wolf, E., Gori, F. and Foley, J.T. (1989) *Journal of the Optical Society of America A*, **6**, 1142-1149. https://doi.org/10.1364/JOSAA.6.001142

[2] Gao, W.R. (2006) *Optics Communications*, **260**, 749-754. https://doi.org/10.1016/j.optcom.2005.10.064

[3] Gao, W.R. and Korotkova, O. (2007) *Optics Communications*, **270**, 474-478. https://doi.org/10.1016/j.optcom.2006.09.061

[4] Gao, W.R. (2010) *Journal of the Optical Society of America A*, **27**, 2588-2592. https://doi.org/10.1364/JOSAA.27.002588

[5] Gao, W.R. (2010) *Optics Letters*, **35**, 862-864. https://doi.org/10.1364/OL.35.000862

[6] Zhu, R., Sridharan, S., Tangella, K., Balla, A. and Popescu, G. (2011) *Optics Letters*, **36**, 4209-4211. https://doi.org/10.1364/OL.36.004209

[7] Gao, W.R. (2013) *Journal of Quantitative Spectroscopy and Radiative Transfer*, **131**, 52-58. https://doi.org/10.1016/j.jqsrt.2013.03.006

[8] Li, J. (2013) *Optics Communications*, **308**, 164-168. https://doi.org/10.1016/j.optcom.2013.06.059

[9] Li, J. and Chang, L.P. (2015) *Optics Express*, **23**, 16602-16616. https://doi.org/10.1364/OE.23.016602

[10] Li, J., Wu, P.H. and Chang, L.P. (2016) *Journal of Quantitative Spectroscopy & Radiative Transfer*, **179**, 126-131. https://doi.org/10.1016/j.jqsrt.2016.03.029

[11] Tong, Z. and Korotkova, O. (2014) *Optics Communications*, **322**, 202-204. https://doi.org/10.1016/j.optcom.2014.02.028

[12] Shchepakina, E., Farwell, N. and Korotkova, O. (2011) *Applied Physics B*, **105**, 415-420. https://doi.org/10.1007/s00340-011-4626-9

[13] Gao, W.R. (2012) *Journal of Microscopy*, **245**, 43-48. https://doi.org/10.1111/j.1365-2818.2011.03542.x

[14] Lahiri, M., Wolf, E., Fischer, D.G. and Shirai, T. (2009) *Physical Review Letters*, **102**, Article ID: 123901. https://doi.org/10.1103/PhysRevLett.102.123901

[15] Yi, J. and Backman, V. (2012) *Optics Letters*, **37**, Article ID: 4443. https://doi.org/10.1364/OL.37.004443

[16] Leitgeb, R., Wojtkowski, M., Kowalczyk, A., Hitzenberger, C.K., Sticker, M. and Fercher, A.F. (2000) *Optics Letters*, **25**, 820-822.

https://doi.org/10.1364/OL.25.000820

[17] Wax, A., Yang, C., Backman, V., Badizadegan, K., Boone, C.W. and Dasari, R.R. (2002) *Biophysical Journal*, **82**, 2256-2264. https://doi.org/10.1016/S0006-3495(02)75571-9

[18] Perelman, L.T., Backman, V., Wallace, M., Zonios, G., Manoharan, R. and Nusrat, A. (1998) *Physical Review Letters*, **80**, 627-630. https://doi.org/10.1103/PhysRevLett.80.627

[19] Backman, V., Wallace, M.B., Perelman, L.T., Arendt, J.T., Gurjar, R. and Müller, M.G. (2000) *Nature*, **406**, 35-36. https://doi.org/10.1038/35017638

[20] Gao, W. (2015) *Proceedings of the Royal Society A*: *Mathematical*, *Physical and Engineering Science*, **471**, 20150099. https://doi.org/10.1098/rspa.2015.0099

[21] Schmitt, J.M. and Kumar, G. (1998) *Applied Optics*, **37**, 2788-2797. https://doi.org/10.1364/AO.37.002788

[22] Sheppard, C.J. (2007) *Optics Letters*, **32**, 142-144.

[23] Schmitt, J.M. and Kumar, G. (1996) *Optics Letters*, **21**, 1310-1312. https://doi.org/10.1364/OL.21.001310

[24] Sheppard, C.J.R. (2006) *Optics Letters*, **32**, 142. https://doi.org/10.1364/OL.32.000142

[25] Beuthan, J., Minet, O., Helfmann, J., Herrig, M. and Müller, G. (1996) *Physics in Medicine & Biology*, **41**, 369-382. https://doi.org/10.1088/0031-9155/41/3/002

[26] Rogers, J.D., Çapoglu Ilker, R. and Backman, V. (2009) *Optics Letters*, **34**, 1891-1893. https://doi.org/10.1364/OL.34.001891

[27] Hunter, M., Backman, V., Popescu, G., Kalashnikov, M., Boone, C.W. and Wax, A. (2006) *Physical Review Letters*, **97**, Article ID: 138102. https://doi.org/10.1103/PhysRevLett.97.138102

[28] Jung, J.H. and Park, Y.K. (2015) *Optics Letters*, **40**, 1093. https://doi.org/10.1364/OL.40.001093

[29] Fercher, A.F., Hitzenberger, C.K., Kamp, G. and El-Zaiat, S.Y. (1995) *Optics Communications*, **117**, 43-48. https://doi.org/10.1016/0030-4018(95)00119-S

[30] Bouma, B.E., Yun, S.H., Vakoc, B.J., Suter, M.J. and Tearney, G.J. (2009) *Current Opinion in Biotechnology*, **20**, 111-118. https://doi.org/10.1016/j.copbio.2009.02.007

[31] Häusler, G. and Lindner, M.W. (1998) *Journal of Biomedical Optics*, **3**, 21. https://doi.org/10.1117/1.429899

[32] Gao, W. and Wu, X. (2017) *Journal of Microscopy*, **268**, 119-128. https://doi.org/10.1111/jmi.12592

[33] Gao, W. (2013) *Journal of Modern Optics*, **60**, 1290-1296. https://doi.org/10.1080/09500340.2013.837977

Journal of Modern Physics, 2019, 10, 452-458
http://www.scirp.org/journal/jmp
ISSN Online: 2153-120X
ISSN Print: 2153-1196

The Linearity of the Euler Equation as a Result of the Compressibility of a Fluid

Vladimir Kirtskhalia[1,2]

[1]I. Vekua Sokhumi Institute of Physics and Technilogy (SIPT), Tbilisi, Georgia
[2]Sokhumi State University, Tbilisi, Georgia
Email: sipt@sipt.org, info@sou.edu.ge

How to cite this paper: Kirtskhalia, V. (2019) The Linearity of the Euler Equation as a Result of the Compressibility of a Fluid. *Journal of Modern Physics*, **10**, 452-458.
https://doi.org/10.4236/jmp.2019.104030

Received: January 20, 2019
Accepted: March 16, 2019
Published: March 19, 2019

Abstract

It is shown that when the compressibility of a fluid is taken into account, the nonlinear term disappears in the Euler equation. The validity of this approach is proved by the example of capillary waves.

Keywords

Euler Equation, Mass Continuity Equation, Fluid Compressibility, Capillary Waves

1. Introduction

In the monography [1], the expression for the square of phase speed of capillary wave on the surface of fluid is received, according to which it generally depends on its depth and consists of the sum of two members. One of them defines the influence of gravitational field, and the second the influence of surface tension, and as a result of which this wave is called capillary-gravitational. This result was obtained under the assumption of the potentiality of motion and incompressibility of a fluid, on which the entire existing theory of gravitational waves is based [2]-[15]. In the work [16] it was shown that the movement of fluid in a gravitational field of the Earth cannot be potential. It was also shown that the condition of incompressibility is inapplicable to liquids, because it leads to the existence of an internal wave [1], the nature of which is completely inexplicable from the point of view of physics. This conclusion was made on the basis of a correct determination of the speed of sound [17] and a new definition of the criteria of compressibility and incompressibility of the medium [18]. This situation made it necessary to refine mass conservation equation, and after its refinement, the gravity acceleration disappeared from the dispersion equation of capil-

lary-gravitational wave, and it becomes purely capillary [16]. The further investigations of gas and hydrodynamics have shown that Euler equation (fluid motion equation) also must be subject to refinement, since for it assumes that the density of a fluid is constant. This approach leads to the fact that the nonlinear term disappears from this equation and it becomes linear.

In this work, we apply Euler's refined equation towards capillary waves and show that despite the use of the boundary condition at the bottom of the liquid, the depth of the reservoir disappears from the dispersion equation, and thus the phase velocity of the capillary wave depends only on its length. In addition, it will be shown that there is no stability condition for a capillary wave, *i.e.* it is always stable in the first equation of system (72) in [16] typo, which the interested reader can easily correct.

2. Improved Euler Equation

In existing gas and hydrodynamics theory, Euler equation is applied in the form:

$$\rho \frac{\mathrm{d}\boldsymbol{V}}{\mathrm{d}t} = \rho\left[\frac{\partial \boldsymbol{V}}{\partial t} + (\boldsymbol{V}\nabla)\boldsymbol{V}\right] = -\nabla P + \rho \boldsymbol{g} \tag{1}$$

where: ρ -density, $\boldsymbol{V}$ —speed fluid particles, P —pressure, $\boldsymbol{g}$ —gravitational acceleration. Here supposed to that liquid is incompressible and consequently $\rho = const$. In several works (see e.g. [19]), it was shown by us, that updated continuity equation of mass has the following form:

$$\frac{\partial \rho}{\partial t} + (\boldsymbol{V}\nabla)\rho = -\rho\nabla\boldsymbol{V} - \frac{\boldsymbol{V}\nabla P}{C_p^2} \tag{2}$$

where C_p is isobaric sound speed in the liquid which can be considered as infinitely large, and we have:

$$\frac{\mathrm{d}\rho}{\mathrm{d}t} = \frac{\partial \rho}{\partial t} + (\boldsymbol{V}\nabla)\rho = -\rho\nabla\boldsymbol{V} \tag{3}$$

From (3) this it follows that liquid is compressible medium ($\nabla\boldsymbol{V} \neq 0$) end $\mathrm{d}\rho/\mathrm{d}t \neq 0$. Consequently, Euler equation should be written in the form of:

$$\frac{\mathrm{d}(\rho\boldsymbol{V})}{\mathrm{d}t} = \boldsymbol{V}\frac{\mathrm{d}\rho}{\mathrm{d}t} + \rho\frac{\mathrm{d}\boldsymbol{V}}{\mathrm{d}t} = -\nabla P + \rho\boldsymbol{g} \tag{4}$$

Then if we substitute $\mathrm{d}\rho/\mathrm{d}t$ from (3) in (4), we get:

$$\begin{aligned} &-\boldsymbol{V}\rho\nabla\boldsymbol{V} + \rho\frac{\mathrm{d}\boldsymbol{V}}{\mathrm{d}t} = -\nabla P + \rho\boldsymbol{g} \\ &\Rightarrow \rho\left[\frac{\mathrm{d}\boldsymbol{V}}{\mathrm{d}t} - (\boldsymbol{V}\nabla)\boldsymbol{V}\right] = -\nabla P + \rho\boldsymbol{g} \\ &\Rightarrow \rho\frac{\partial \boldsymbol{V}}{\partial t} = -\nabla P + \rho\boldsymbol{g} \end{aligned} \tag{5}$$

So, we have a system of two equations:

$$\begin{cases} \rho \dfrac{\partial \boldsymbol{V}}{\partial t} = -\nabla P + \rho \boldsymbol{g} \\ \dfrac{\partial \rho}{\partial t} + (\boldsymbol{V}\nabla)\rho = -\rho \nabla \boldsymbol{V} \end{cases} \tag{6}$$

We see that the nonlinear term from the Euler equation has disappeared. It remains only in the mass conservation equation.

3. Dispersion Equation of Capillary Waves and Her Decision

Let's presenting all the variables from the system (6) in the form of the sum of their stationary and perturbed values $f = f_0 + f'$ and supposing that $f'/f_0 < 1$, after linearization it will take the following form:

$$\begin{cases} \rho_0 \dfrac{\partial V}{\partial t} = -\nabla P + \dfrac{\boldsymbol{g}}{C^2} P \\ \dfrac{1}{C^2}\left(\dfrac{\partial P}{\partial t} + \boldsymbol{V}_0 \nabla P\right) = -\rho_0 \nabla \boldsymbol{V} \end{cases} \tag{7}$$

where we used: state equation of medium $\rho' = P'/C^2$ (C—adiabatic speed of sound in the liquid), liquid equilibrium equation $\nabla P_0 = \rho_0 \boldsymbol{g}$ and perturbed values don't have stokes.

If $\bar{V}_0$ there is a stationary velocity of fluid flow, then the linearized Equation (1) will be

$$\rho_0 \left[\frac{\partial \boldsymbol{V}}{\partial t} + (\boldsymbol{V}_0 \nabla)\boldsymbol{V}\right] = -\nabla P + \frac{\boldsymbol{g}}{C^2} P$$

As we see, this equation, which determines the acceleration of a liquid particle, contains a stationary velocity of motion, on which the acceleration should not depend. This fact irrefutably proves the validity of formula (4).

Appling to the first equation of system (7) operator ∇ and to the second operator $\partial/\partial t$, they easily reduced to differential equation for perturbed pressure

$$\Delta P - \frac{1}{C^2}\left(\vec{g} + \vec{V}_0 \frac{\partial}{\partial t}\right)\nabla P - \frac{1}{C^2}\frac{\partial^2 P}{\partial t^2} = 0 \tag{8}$$

Presenting now the perturbed pressure in the form of periodic function

$$P(x, z, t) = P_a(z)\exp\left[i(kx - \omega t)\right] \tag{9}$$

and supposing that $\boldsymbol{V}_0 = \boldsymbol{e}_x V_0$ and $\boldsymbol{g} = -\boldsymbol{e}_z g$, we will get ordinary differential equation of second order for the amplitude of pressure disturbance in the following form:

$$\frac{\mathrm{d}^2 P_a(z)}{\mathrm{d}z^2} + \frac{g}{C^2}\frac{\mathrm{d}P_a(z)}{\mathrm{d}z} + \left[\frac{\omega}{C^2}(\omega - kV_0) - k^2\right]P_a(z) = 0 \tag{10}$$

The Equation (10) describes pressure disturbance on both sides of surface of tangential discontinuity $z = 0$. We solve this equation for air $(z > 0)$ in the form:

$$P_{a1}(z) = A\exp(\gamma z), \tag{11}$$

where upon, taking into account the attenuation of the disturbance when $z \to \infty$, for γ we will get:

$$\gamma = -\frac{k}{\theta_1}\left\{1+\sqrt{1+\theta_1^2\left[1-\frac{U_p(U_p-V_0)}{C_1^2}\right]}\right\} < 0 \tag{12}$$

where C_1 is sound speed in the air on the sea level, $U_p = \omega/k$ is phase speed of surface wave and θ_1 is dimensionless value and it is equal to

$$\theta_1 = \frac{2kC_1^2}{g} \tag{13}$$

For the liquid $(z<0)$, because of its depth limitation, from (10) analogically we will have:

$$P_{a2}(z) = B_1\exp(\delta_1 z) + B_2\exp(\delta_2 z) \tag{14}$$

where

$$\delta_1 = -\frac{k}{\theta_2}\left[1+\sqrt{1+\theta_2^2\left(1-\frac{U_p^2}{C_2^2}\right)}\right] < 0 \tag{15}$$

$$\delta_2 = -\frac{k}{\theta_2}\left[1-\sqrt{1+\theta_2^2\left(1-\frac{U_p^2}{C_2^2}\right)}\right] > 0 \tag{16}$$

$$\theta_2 = \frac{2kC_2^2}{g} \tag{17}$$

Let us denote liquid surface displacement along the axis z through

$$\xi(x,t) = a\exp\left[i(kx-\omega t)\right] \tag{18}$$

and in this case, the boundary conditions on the surface $(z=0)$ and on the bottom $(z=-h)$ of the liquid will have the form of:

$$\begin{cases} (P_2-P_1)\big|_{z=0} = -\alpha\dfrac{\partial^2\xi}{\partial x^2} \\ V_{z1}\big|_{z=0} = \dfrac{\partial\xi}{\partial t} + V_0\dfrac{\partial\xi}{\partial x} \\ V_{z2}\big|_{z=0} = \dfrac{\partial\xi}{\partial t} \\ V_{z2}\big|_{z=-h} = 0 \end{cases} \tag{19}$$

where α is the coefficient of surface tension.

Let's present perturbation velocity in the form of periodical function:

$$\boldsymbol{V}(x,z,t) = \boldsymbol{V}_a(z)\exp\left[i(kx-\omega t)\right] \tag{20}$$

and denote its z component through disturbance pressure from the first equation of the system (7):

$$V_z(x,z,t) = -\frac{i}{\rho_0\omega}\left[\frac{\partial P_a(z)}{\partial z} + \frac{g}{C^2}P_a(z)\right]\exp\left[i(kx-\omega t)\right] \tag{21}$$

Substituting (9), (11), (14) and (21) in the boundary conditions (19), we will get the system of homogenous equations referred to unknown coefficients A, B_1, B_2 and a:

$$\begin{cases} A - B_1 - B_2 + \alpha k^2 a = 0 \\ \dfrac{\gamma + g/C_1^2}{\rho_{01}\omega}A - (\omega - kV_0)a = 0 \\ \dfrac{\delta_1 + g/C_2^2}{\rho_{02}\omega}B_1 + \dfrac{\delta_2 + g/C_2^2}{\rho_{02}\omega}B_2 - \omega a = 0 \\ \dfrac{\delta_1 + g/C_2^2}{\rho_{02}\omega}\exp(-\delta_1 h)B_1 + \dfrac{\delta_2 + g/C_2^2}{\rho_{02}\omega}\exp(-\delta_2 h)B_2 = 0 \end{cases} \tag{22}$$

Equating the determinant of the system (22) to zero, we will get dispersion relation for the wave on the liquid surface taking into account surface tension force in the form of:

$$\begin{aligned} &\frac{\delta_1\delta_2}{\rho_{02}\omega}\left(\omega - kV_0 - \frac{\gamma}{\rho_{01}\omega}\alpha k^2\right)\left[\exp(-\delta_1 h) - \exp(-\delta_2 h)\right] \\ &-\frac{\gamma}{\rho_{01}}\left[\delta_2\exp(-\delta_1 h) + \delta_1\exp(-\delta_2 h)\right] = 0 \end{aligned} \tag{23}$$

Taking into account that on the sea level $C_1 \cong 340$ m/sec, let's consider the inequality

$$\theta_1 = \frac{2kC_1^2}{g} > 1 \Rightarrow k > \frac{g}{2C_1^2} \Rightarrow \lambda < \frac{4\pi C_1^2}{g} = 1.45\times 10^5 \text{ m}$$

We can see, that to this inequality satisfies with the entire range of lengths of surface waves on the water, from capillary to tsunami. It is apparent that for the capillary waves length of which does not exceed a few centimeters, we have: $\theta_2 \gg \theta_1 \gg 1$. Considering also that $U_p^2/C_2^2 \ll U_p^2/C_1^2 \ll 1$, from (12), (15) and (16) we find $\gamma = \delta_1 = -k$, $\delta_2 = k$ and then neglecting ρ_{01} with respect to ρ_{02}, the dispersion Equation (23) takes the form:

$$\rho_{02}U_p^2 + \rho_{01}V_0U_p - \alpha k = 0 \tag{24}$$

the solution of which is

$$U_p = \frac{-\rho_{01}V_0 \pm \sqrt{\rho_{01}^2V_0^2 + 4\alpha k\rho_{02}}}{2\rho_{02}} \tag{25}$$

4. Discussion of Results

In order to show the truthfulness of our results, let's consider earlier results and show their drawbacks. As it was said in the introduction, in the monography [1] dispersion relation for the capillary-gravitational wave on the surface of incompressible liquid is presented in the form of:

$$U_p^2 = \left(\frac{\omega}{k}\right)^2 = \left(\frac{g}{k} + \frac{\alpha k}{\rho_{02}}\right) th(kh) \tag{26}$$

from which it follows that when

$$\frac{g}{k} > \frac{\alpha k}{\rho_{02}} \Rightarrow k < \sqrt{\frac{\rho_{02} g}{\alpha}} \Rightarrow \lambda > 2\pi\sqrt{\frac{\alpha}{\rho_{02} g}} = 1.72 \text{ sm} \tag{27}$$

the influence of the surface tension force is negligible, and the wave becomes purely gravitational. This conclusion contradicts to the classical experiment, in which a steel needle does not sink in a glass filled with water to the brim. This is because although the diameter of glass greatly exceeds the above specified length, the force of surface tension acts which balances the pressure produced by the needle. Thus, the dependence of phase speed on gravitational acceleration is excluded and consequently there is no existing condition that limits the length of capillary wave. Such a conclusion is quite understandable from the point of view of physics, because surface tension arises due to the interaction forces between molecules on the surface of a liquid that significantly exceed the gravitational force.

The contradiction associated with the influence of the gravitational field is eliminated by taking into account the compressibility of the fluid in the mass continuity equation. The solution of the problem for such a case is given in [17], where the dispersion equation is obtained in the form:

$$U_p = \frac{\omega}{k} = \frac{\rho_{01} V_0 th(kh) \pm \left\{ th(kh)\left[\rho_{02}\alpha k - \rho_{01}\rho_{02} V_0^2\right]\right\}^{1/2}}{\rho_{02}} \tag{28}$$

from which follows the condition of stability of capillary wave:

$$V_0 \le \sqrt{\frac{\alpha k}{\rho_{01}}} \tag{29}$$

From (29) it is easy to calculate that the wind with the speed of $V_0 = 5$ m/s, will blow off capillary waves whose length $\lambda > 1.6$ cm. However, simple observations show that capillary waves exist at quite stronger winds. In addition, since the capillary wave is a purely surface phenomenon, its phase speed must not depend on the depth of the fluid.

As it is apparent in the Equation (25), this contradiction is eliminated if in Euler equation, we consider liquid as compressible. Capillary wave is stable in any wind, if only the wind force does not exceed intermolecular interaction force and in this case, setting of the problem becomes meaningless. We can also see that phase speed of capillary wave does not depend on the depth of fluid.

5. Conclusion

Contradictions that are present in the theory of surface waves are described in detail in the works [16] and [19]. In this work, through the example of capillary waves we have explicitly investigated the causes of these contradictions and showed how to overcome them. We can say with confidence that our recom-

mendations will result in overcoming contradictions not only in the theory of capillary waves but also in the theory of gravity waves too.

Conflicts of Interest

The author declares no conflicts of interest regarding the publication of this paper.

References

[1] Landau, L.D. and Lifshitz, E.N. (1988) *Hydrodynamics*, Vol. 6, Nauka, Moscow.

[2] Stoker, J.J. (1957) Water Waves. Intersciense Publisher Inc., New York.

[3] Whitham, G. (1974) Linear and Nonlinear Waves. John Wiley and Sons, Hoboken.

[4] Kowalik, Z. (2012) Introduction to Numerical Modeling of Tsunami Waves. Institute of Marine Science University of Alaska, Fairbank.

[5] Hassan, J.M., Mohamed, T.A., Mohammed, W.S. and Alawee, W.H. (2014) *Journal of Fluids*, **2014**, Article ID: 325259.

[6] Chand, R. and Rana, G.C. (2014) *Journal of Fluids*, **2014**, Article ID: 479107.

[7] Rabby, M.G., Shupti, S.P. and Molla, M.M. (2014) *Journal of Fluids*, **2014**, Article ID: 757902. https://doi.org/10.1155/2014/757902

[8] Eldabe, N.T.M., Agoor, B.M. and Alame, H. (2014) *Journal of Fluids*, **2014**, Article ID: 525769.

[9] Singh, M. and Gupta, R.K. (2014) *Journal of Fluids*, **2014**, Article ID: 714150.

[10] Troshkin, O. (2016) *Mathematics and Statistics*, **4**, 47-57. https://doi.org/10.13189/ms.2016.040201

[11] Campos Pinto, M. and Charles, F. (2016) *Proceedings and Surveys*, **53**, 38-48. https://doi.org/10.1051/proc/201653003

[12] Cotter, C.J., Eldering, J., Holm, D.D., Jacobs, H.O. and Meier, D.M. (2016) *Journal of Nonlinear Science*, **26**, 723-765. https://doi.org/10.1007/s00332-016-9317-6

[13] Cubos-Ramírez, J.M., Ramírez-Cruz, Salinas-Vázquez, J.M., Vicente-Rodríguez, W., Martinez-Espinosa, E. and Lagarza-Cortes, C. (2016) *Computers & Fluids*, **136**, 212-227.

[14] Rehman, K. and Cho, Y. (2016) *Water*, **8**, 212. https://doi.org/10.3390/w8050212

[15] Ogilvie, G.I. (2016) *Journal of Plasma Physics*, **82**, 212. https://doi.org/10.1017/S0022377816000489

[16] Kirtskhalia, V. (2016) *Journal of Fluids*, **2016**, Article ID: 4519201. https://doi.org/10.1155/2016/4519201

[17] Kirtskhalia, V. (2012) *Open Journal of Acoustics*, **2**, 80-85. https://doi.org/10.4236/oja.2012.22009

[18] Kirtskhalia, V. (2013) *Journal of Modern Physics*, **4**, 1075-1079. https://doi.org/10.4236/jmp.2013.48144

[19] Kirtskhalia, V. (2015) Applied Problems of Gas and Hydrodynamics. Academic Publishing "LAMBERT", Saarbrucken.

Journal of Modern Physics, 2019, 10, 459-465
http://www.scirp.org/journal/jmp
ISSN Online: 2153-120X
ISSN Print: 2153-1196

An Evanescent Light Wave Cannot Possess a Transverse Spin

Chunfang Li, Yunlong Zhang

Department of Physics, Shanghai University, Shanghai, China
Email: cfli@shu.edu.cn

How to cite this paper: Li, C.F. and Zhang, Y.L. (2019) An Evanescent Light Wave Cannot Possess a Transverse Spin. *Journal of Modern Physics*, **10**, 459-465.

https://dx.doi.org/10.4236/jmp.2019.104031

Received: February 28, 2019
Accepted: March 19, 2019
Published: March 22, 2019

Abstract

It is pointed out that the evanescent light wave occurring at total reflection does not possess a transverse spin angular momentum as Bliokh, Bekshaev, and Nori claimed recently in (2014) *Nature Communications*, **5**, 3300. This is not only because of the nonlocality of the photon spin but also because the evanescent wave is such a state whose angular momentum cannot be separated into spin and orbital parts.

Keywords

Nonexistence, Transverse Spin, Evanescent Light Wave

1. Introduction

It was once believed [1] [2] that separating the photon angular momentum into its spin and orbital parts is physically meaningless. However, since the seminal work of Allen *et al.* [3], theoretical identification of spin and orbital parts of photon angular momentum have drawn much attention [4–14]. In a recent publication, Bliokh, Bekshaev, and Nori [15] claimed that the evanescent light wave occurring at total reflection has a transverse spin, which is independent of the polarization. They arrived at that conclusion by resorting to the so-called local densities for the spin and orbital angular momentum (OAM), which were constructed in Ref. [11].

Bialynicki-Birula [12] showed that even though the total angular momentum of a light wave is local, after the splitting into spin and orbital parts, "the locality is lost". Furthermore, one of the authors [16] found that the spin of the photon can be derived from a set of two relativistic quantum equations for those states with respect to which the momentum operator is Hermitian. The nonlocality of the photon spin originates in the nonlocality of the photon itself that is expressed by the relativistic quantum constraint. On the basis of these discussions, we will demonstrate in this paper that the notion of transverse spin advanced in Ref. [15] is physically incorrect.

2. Description of Demonstration Method

For clarity, let us first take a brief look at how Bliokh *et al.* came to their conclusion. Consider a monochromatic light wave of angular frequency ω in the air. The local spin density they defined reads

$$\boldsymbol{s} = \psi^\dagger \hat{\boldsymbol{S}} \psi = \frac{\gamma}{2}\mathrm{Im}(\boldsymbol{E}^* \times \boldsymbol{E} + \boldsymbol{H}^* \times \boldsymbol{H}), \tag{1}$$

where $\hat{\boldsymbol{S}} = \begin{pmatrix} \hat{\boldsymbol{\Sigma}} & 0 \\ 0 & \hat{\boldsymbol{\Sigma}} \end{pmatrix}$ is a vector matrix, $(\hat{\Sigma}_k)_{ij} = -i\epsilon_{ijk}$ with ϵ_{ijk} the Levi-Civitá pseudotensor, $\psi = \sqrt{\frac{\gamma}{2}}\begin{pmatrix} \boldsymbol{E} \\ \boldsymbol{H} \end{pmatrix}$ is the spinor wavefunction with $\boldsymbol{E}$ and $\boldsymbol{H}$ the complex electric and magnetic vectors, respectively, the superscript "†" denotes the conjugate transpose, the superscript "$*$" denotes the complex conjugate, Gaussian units with $\gamma = (8\pi\omega)^{-1}$ are used, and $\hbar = 1$ is assumed. They claimed that the spin density is generated by the so-called spin part $\boldsymbol{p}^S$ of the momentum density in the following way,

$$\boldsymbol{s} = \boldsymbol{x} \times \boldsymbol{p}^S, \tag{2}$$

where $\boldsymbol{x}$ is the position vector relative to the origin. Meanwhile, they claimed that $\boldsymbol{p}^S$ is expressed in terms of $\boldsymbol{s}$ as

$$\boldsymbol{p}^S = \frac{1}{2}\nabla \times \boldsymbol{s}. \tag{3}$$

The local OAM density about the origin they defined is as follows,

$$\boldsymbol{l} = \boldsymbol{x} \times \boldsymbol{p}^O, \tag{4}$$

where

$$\boldsymbol{p}^O = \mathrm{Re}(\psi^\dagger \hat{\boldsymbol{P}} \psi) = \frac{\gamma}{2}\mathrm{Im}[(\nabla \boldsymbol{E}) \cdot \boldsymbol{E}^* + (\nabla \boldsymbol{H}) \cdot \boldsymbol{H}^*] \tag{5}$$

is the so-called canonical part of the momentum density and $\hat{\boldsymbol{P}} = -i\nabla$ is the operator for the canonical momentum. They required that the sum of $\boldsymbol{p}^S$ and $\boldsymbol{p}^O$ should be equal to the momentum density that is proportional to the Poynting vector and is expressed in terms of the complex electric and magnetic vectors as

$$\boldsymbol{p} = \gamma k_0 \mathrm{Re}(\boldsymbol{E}^* \times \boldsymbol{H}), \tag{6}$$

where $k_0 = \omega/c$ is the wavenumber in the air. When applying Equation (1) to the evanescent wave that occurs at a total reflection, they found that $\boldsymbol{s}$ is perpendicular to the propagation direction.

It is well known [17] [18] [19] that the angular momentum of a light wave about the origin is given by $\int \boldsymbol{x} \times \boldsymbol{p} d^3x$, where the integrand is known as the angular-momentum density about the origin,

$$\boldsymbol{j} = \boldsymbol{x} \times \boldsymbol{p}, \tag{7}$$

and $\boldsymbol{p}$ is the momentum density (6). As a physically meaningful notion, the angular-momentum density has to be unique. So if $\boldsymbol{s}$ in Equation (1) and $\boldsymbol{l}$ in Equation (4) are true local spin and OAM densities, respectively, one must have $\boldsymbol{s} + \boldsymbol{l} = \boldsymbol{j}$. This can also be seen from $\boldsymbol{p}^S + \boldsymbol{p}^O = \boldsymbol{p}$ if $\boldsymbol{s}$ is generated by $\boldsymbol{p}^S$ via Equation (2). To demonstrate the nonexistence of the transverse spin in an evanescent wave, it is enough to show that there is no such relation in that case. This is done below.

3. Demonstration of Nonexistence of the Transverse Spin

Because it was claimed in Ref. [15] that the transverse spin in an evanescent wave is independent of the polarization, we consider such an evanescent wave that occurs when a TM-polarized plane wave is totally reflected by an interface between a dielectric medium of refractive index $n_i > 1$ and the air of refractive index $n_0 = 1$ as is shown in Figure 1.

The complex magnetic vector of the evanescent wave in the air assumes the following form,

$$\boldsymbol{H} = A\exp[i(\boldsymbol{k}_0 \cdot \boldsymbol{x} - \omega t)]\bar{y}, \quad x \geq 0, \tag{8}$$

where A is a constant, $\boldsymbol{k}_0 = i\kappa\bar{x} + k_z\bar{z}$ is the complex wavevector, $\kappa = (k_z^2 - k_0^2)^{1/2}$ is the decay coefficient in the air, $k_z = k_i \sin\theta$, $k_i = n_i k_0$, θ is the incidence angle that is larger than the critical angle for total reflection $\theta_c = \sin^{-1}(1/n_i)$, $\bar{x}$, $\bar{y}$, and $\bar{z}$ are unit vectors along the corresponding axes. The corresponding complex electric vector is given by

$$\boldsymbol{E} = \frac{k_z\bar{x} - i\kappa\bar{z}}{k_0} A\exp[i(\boldsymbol{k}_0 \cdot \boldsymbol{x} - \omega t)], \quad x \geq 0. \tag{9}$$

It is needless to say that the electric vector (9) is "perpendicular" to the associated complex wavevector, $\boldsymbol{E} \cdot \boldsymbol{k}_0 = 0$, as the Maxwell equation $\nabla \cdot \boldsymbol{E} = 0$ requires. Substituting Equations (8) and (9) into Equation (6), we find for the momentum density,

$$\boldsymbol{p} = \gamma k_z |A|^2 \exp(-2\kappa x)\bar{z}, \tag{10}$$

which is in the propagation direction, the z-axis. Upon substituting it into Equation (7), we have for the angular-momentum density about the origin,

$$\boldsymbol{j} = \gamma k_z |A|^2 \exp(-2\kappa x)(y\bar{x} - x\bar{y}). \tag{11}$$

It is transverse, having both x and y components.

Substituting Equations (8) and (9) into Equation (1), one gets

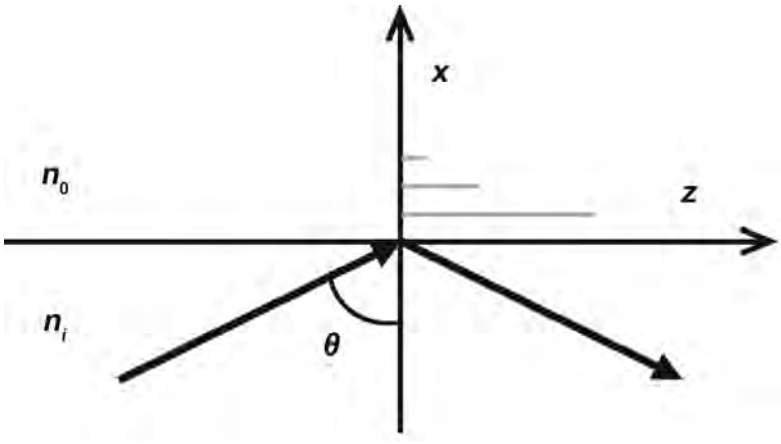

Figure 1. The evanescent wave that occurs at the total reflection of a TM-polarized plane wave by an interface at $x = 0$ between two dielectric media of refractive indices n_i and n_0.

$$\boldsymbol{s} = \frac{\gamma k_z \kappa}{k_0^2}|A|^2 \exp(-2\kappa x)\bar{y}, \tag{12}$$

which is in the transverse y direction. It is on the basis of this result that Bliokh *et al.* [15] claimed that the evanescent wave possesses a transverse spin. However, substituting Equations (8) and (9) into Equation (5), one finds

$$\boldsymbol{p}^O = \frac{\gamma k_z^3}{k_0^2}|A|^2 \exp(-2\kappa x)\bar{z}, \tag{13}$$

which, when substituted into Equation (4), gives

$$\boldsymbol{l} = \frac{\gamma k_z^3}{k_0^2}|A|^2 \exp(-2\kappa x)(y\bar{x} - x\bar{y}). \tag{14}$$

Obviously, the sum of $\boldsymbol{s}$ and $\boldsymbol{l}$ in Equations (12) and (14) is different from the angular-momentum density (11). Instead, one has

$$\boldsymbol{s} + \boldsymbol{l} = \frac{\gamma k_z}{k_0^2}|A|^2 \exp(-2\kappa x)[k_z^2 y\bar{x} + (\kappa - k_z^2 x)\bar{y}].$$

From this result it is concluded that the $\boldsymbol{s}$ in Equation (12) cannot be the local spin density and therefore the evanescent light wave does not possess a transverse spin.

Furthermore, substituting Equation (12) into Equation (3), one has

$$\boldsymbol{p}^S = -\frac{\gamma k_z \kappa^2}{k_0^2}|A|^2 \exp(-2\kappa x)\bar{z}. \tag{15}$$

The sum of (13) and (15) is indeed equal to the momentum density (10). But upon substituting Equation (15) into Equation (2), one cannot find Equation (12). Instead, one obtains

$$\boldsymbol{x} \times \boldsymbol{p}^S = -\frac{\gamma k_z \kappa^2}{k_0^2}|A|^2 \exp(-2\kappa x)(y\bar{x} - x\bar{y}), \tag{16}$$

which, in addition to a y-component, has a x-component. This is understandable. Resulting from Equation (1), the $\boldsymbol{s}$ in Equation (12) is supposed to be independent of the choice of a reference point. Nevertheless, coming from Equation (2), expression (16) must depend on the reference point, the origin. This further demonstrates that the $\boldsymbol{s}$ in Equation (12) is not the local spin density. After all, as pointed out by Bialynicki-Birula [12], "when one splits the total angular momentum into its orbital part and the intrinsic part, locality cannot be preserved".

It is noted that according to the definition in quantum mechanics [20], the expectation value of the canonical momentum taken with respect to state ψ is given by

$$\langle \hat{\boldsymbol{P}} \rangle = \frac{\int \psi^\dagger \hat{\boldsymbol{P}} \psi d^3x}{\int \psi^\dagger \psi d^3x}.$$

If the evanescent wave (8) and (9) can be regarded as a photon state, the resultant expectation value of the canonical momentum is complex, $\langle \hat{\boldsymbol{P}} \rangle = \boldsymbol{k}_0 = i\kappa\bar{x} + k_z\bar{z}$. This shows that the evanescent wave is such a state with respect to which the canonical-momentum operator is not Hermitian. In other words, the canonical momentum of

the photon in the evanescent wave is not an observable from the point of view of quantum mechanics. Accordingly, the corresponding OAM represented by the operator $\boldsymbol{x} \times \hat{\boldsymbol{P}}$ is not an observable, either. As a consequence, dividing the angular momentum of the photon in the evanescent wave into spin and orbital parts is physically impossible. This also explains why the angular momentum density $\boldsymbol{j}$ given by Equation (11) is different from the sum of $\boldsymbol{s}$ and $\boldsymbol{l}$ in Equations (12) and (14).

4. Discussions and Conclusions

On a final note, the photon in the evanescent wave (8) and (9) does have a transverse angular momentum about the origin. To see this in more detail, let us calculate the energy density of the evanescent wave,

$$u = \frac{1}{16\pi}(|\boldsymbol{E}|^2 + |\boldsymbol{H}|^2) = \frac{k_z^2}{8\pi k_0^2}|A|^2 \exp(-2\kappa x).$$

Considering that the energy of each photon is ω, we adopt the technique used in Ref. [6] to find the momentum of a single photon per unit length along the propagation direction,

$$\boldsymbol{P} = \omega \frac{\int_{x\geq 0} \boldsymbol{p} dxdy}{\int_{x\geq 0} u dxdy} = \frac{k_0^2}{k_z}\bar{z}.$$

Because of $\frac{k_0}{k_z} < 1$, its magnitude, $P = \frac{k_0^2}{k_z}$, is less than that of the momentum of free photon in the air, k_0. Correspondingly, from Equation (11) we have for the angular momentum of a single photon per unit length along the propagation direction,

$$\boldsymbol{J} = \omega \frac{\int_{x\geq 0} \boldsymbol{j} dxdy}{\int_{x\geq 0} u dxdy} = -\frac{P}{2\kappa}\bar{y},$$

which is in the transverse y direction. According to the definition of the angular momentum of a point particle about the origin, $\boldsymbol{J} = \boldsymbol{x} \times \boldsymbol{P}$, it follows from preceding two equations that the x-component of the photon's position vector $\boldsymbol{x}$ at any instant is $x = \frac{1}{2\kappa}$ if we consider the photon as a point particle. That is to say, the photon behaves as a point particle of momentum P along the propagation direction with a distance $\frac{1}{2\kappa}$ away from the interface. The effect of such a transverse angular momentum was observed twenty years ago [21] in an experiment on combined Mie particles and was then explained as the result of the vertical gradient of the longitudinal radiation pressure that is expressed by the momentum density (10).

In conclusion, the evanescent light wave does not possess a transverse spin not only because of the nonlocality of the photon spin but also because the angular momentum of the evanescent wave cannot be separated into spin and orbital parts.

Acknowledgements

This work was supported in part by the program of Shanghai Municipal Science and Technology Commission (18ZR1415500).

Conflicts of Interest

The authors declare no competing financial interests.

References

[1] Akhiezer, A.I. and Berestetskii, V.B. (1965) Quantum Electrodynamics. Interscience, New York.

[2] Cohen-Tannoudji, C., Dupont-Roc, J. and Grynberg, G. (1989) Photons and Atoms. John Wiley & Sons, New York.

[3] Allen, L., Beijersbergen, M.W., Spreeuw, R.J.C. and Woerdman, J.P. (1992) *Physical Review A*, **45**, 8185-8189. https://doi.org/10.1103/PhysRevA.45.8185

[4] van Enk, S.J. and Nienhuis, G. (1994) *Europhysics Letters*, **25**, 497-501. https://doi.org/10.1209/0295-5075/25/7/004

[5] van Enk, S.J. and Nienhuis, G. (1994) *Journal of Modern Optics*, **41**, 963-977. https://doi.org/10.1080/09500349414550911

[6] Barnett, S.M. and Allen, L. (1994) *Optics Communications*, **110**, 670-678. https://doi.org/10.1016/0030-4018(94)90269-0

[7] Barnett, S.M. (2002) *Journal of Optics B: Quantum and Semiclassical Optics*, **4**, S7-S16. https://doi.org/10.1088/1464-4266/4/2/361

[8] Barnett, S.M. (2010) *Journal of Modern Optics*, **57**, 1339-1343. https://doi.org/10.1080/09500341003654427

[9] Li, C.-F. (2009) *Physical Review A*, **80**, Article ID: 063814.

[10] Li, C.-F. (2016) *Physical Review A*, **93**, Article ID: 049902(E).

[11] Bliokh, K.Y., Dressel, J. and Nori, F. (2014) *New Journal of Physics*, **16**, Article ID: 093037. https://doi.org/10.1088/1367-2630/16/9/093037

[12] Bialynicki-Birula, I. (2014) *New Journal of Physics*, **16**, Article ID: 113056. https://doi.org/10.1088/1367-2630/16/11/113056

[13] Barnett, S.M., Allen, L., Cameron, R.P., Gilson, C.R., Padgett, M.J., Speirits, F.C. and Yao, A.M. (2016) *Journal of Optics*, **18**, Article ID: 064004.

[14] Leader, E. (2018) *Physics Letters B*, **779**, 385-387. https://doi.org/10.1016/j.physletb.2018.02.029

[15] Bliokh, K.Y., Bekshaev, A.Y. and Nori, F. (2014) *Nature Communications*, **5**, Article No. 3300. https://doi.org/10.1038/ncomms4300

[16] Li, C.-F. (2019) Deriving Photon Spin from Relativistic Quantum Equations: Relativistic Quantum Constraint and Nonlocality of Photon Spin. arXiv:1806.04540v2

[17] Stratton, J.A. (1941) Electromagnetic Theory. McGraw-Hill, New York.

[18] Mandel, L. and Wolf, E. (1995) Optical Coherence and Quantum Optics. Cambridge University Press, Cambridge. https://doi.org/10.1017/CBO9781139644105

[19] Jackson, J.D. (1999) Classical Electrodynamics. 3rd Edition. John Wiley & Sons, New York.

[20] Sakurai, J.J. (1985) Modern Quantum Mechanics. Benjamin/Cummings, San Francisco, CA.

[21] Song, Y.G., Chang, S. and Jo, J.H. (1999) *Japanese Journal of Applied Physics*, **38**, L380-L383. https://doi.org/10.1143/JJAP.38.L380

Journal of Modern Physics, 2019, 10, 466-476
http://www.scirp.org/journal/jmp
ISSN Online: 2153-120X
ISSN Print: 2153-1196

Values of Siva's Constant "*K*" for All Fundamental Forces—A Review on Spin, Threshold Time and Quantum Entanglement

Siva Prasad Kodukula

Visakhapatnam, India
Email: sivkod@gmail.com

How to cite this paper: Kodukula, S.P. (2019) Values of Siva's Constant "*K*" for All Fundamental Forces—A Review on Spin, Threshold Time and Quantum Entanglement. *Journal of Modern Physics*, **10**, 466-476.
https://doi.org/10.4236/jmp.2019.104032

Received: February 25, 2019
Accepted: March 19, 2019
Published: March 22, 2019

Abstract

Siva's constant "*K*" has been explained in brief. Its numerical values have been calculated for each fundamental force of nature. Spin of quantum mechanics has been interpreted in terms of Sivas constant "*K*". Thus limitation to velocity of light and interrelation between relativity and quantum mechanics has been explained in a novel and profound way. Involvement of "physics of consciousness" in synchronizing relativity and quantum mechanics has been emphasized. Concept of "bio force" as fifth fundamental force in addition to other four fundamental forces, strong, weak, electromagnetic and gravitational forces also has been emphasized. Consciousness has been explained as entanglement between bio force particle named as "jeeton" and gravitational force particle "graviton". Thus frequency mediated consciousness has been explained.

Keywords

Siva's Constant "*K*", Bio Force Particle, Jeeton, Spin, Grand Unification, Quantum Mechanics, Relativity, Quantum Entanglement

1. Introduction

Sivas constant "*K*" is introduced in "Double relativity Effect". In that, it is postulated that the universe is existed with absolute velocities. There is an absolute velocity at a distance "*d*" from any point of observation in space time and it is proportional to distance "*d*". Proportionality constant is "Hubble's constant" "*H*" and follows by an equation $V = Hd$. It represents the "expansion" explained by the Hubble's concept of "expanding universe". Due to "Double Relativity Effect", as the velocity increases with distance the same force of expansion will be ex-

pressed as gravity force and will be denoted by $Vd = K$, where "K" is Siva's constant. In both the cases, absolute velocity is observed as "observed velocity" due to the fact that universe is existed as films as explained in the papers [1] [2] [3].

By considering the diameter of the universe as diameter of hydrogen atom which is the smallest atom representing matter, Siva's Constant has been calculated as 2×10^2 sqmt/sec [2]. Later when it is applied to relativity and quantum mechanics it is realized that it is a major mistake with erroneous calculations and reconsidered the concept that all the relative velocities are consequences of absolute velocities and explained as films explained in "film theory of the universe" [3]. As per this concept, the events of this universe are part of "film change" of this universe. It is postulated that the duration of film change is "plank time". This has been elaborated in the paper [3]. Thus it is explained that absolute velocity associated to a film will be converted into acceleration during film change of the universe. This acceleration is the cause for gravitational force. Thus the postulated equation $Vd = K$ is applied to the concept of gravitation and derived an equation for gravitation with Siva's constant "K" [4]. The same principle has been adopted to define other three fundamental forces. The concept has been elaborated in the paper [5]. It is explained that "space time" is the main cause for all fundamental forces and can be explained by same equations and achieved grand unification. But "K" is not a constant. It will vary with density of "space time" and the fundamental force. These grand unification equations described an equation relating "space-time diameter" and "coupling constant" of fundamental forces. "Space-time diameter" is dependent on parameter "K".

But in lot of previous works "K" has been considered as a non varying constant *i.e.* 2×10^2 sqmt/sec [1] [2] [6] [7] [8] [9] [10]. All those concepts have been reconsidered and concluded the concepts with recalculated values according to the change of "K". Application of these corrections to the paper [6] has concluded that "bio-force" which is a force existed in all living things is also a fundamental force. Example for this force is the force utilized to lift the parts of the body against to gravity. It can be claimed as "fifth force". The other four fundamental forces are strong force, weak interaction, electromagnetic force and gravitational force. Research is in process to unify all these fundamental forces. Already a new approach has been explained the paper "Plank Scale with Siva's Constant "K"—A New Road to Grand Unification" [5] based on space, time and "space-time" concepts. In All these forces and their interactions Siva's constant "K" plays a crucial role. "K" value for all fundamental forces including "bio force" has been calculated and tabulated along with the concerned coupling constants mentioned in "standard model". Now "K" will become a necessary parameter in addition to G, c, h and $\hbar$ to understand the "plank scale" in a full pledged manner.

Inter relation between these parameters will explain the five fundamental

forces including "bio force" and their unification. Surprisingly these equations with interchange of these parameters showed a path way to explain most fundamental concepts of quantum mechanics such as "spin", "threshold time" and "quantum entanglement" between two separate force particles.

2. Calculation of "*K*" Values for All Fundamental Forces

Siva's constant "*K*" can be calculated by Siva's equations for grand unification. The third equation shows the relation between "space time diameter" of quantum of fundamental force and the coupling constant with respect to electromagnetic force. We have coupling constants for three fundamental forces *i.e.* strong force, electromagnetic force and weak interactions as per "standard model". We do not have perfect grand unification theory for unification of gravity with other three forces. So from the fundamentals we have calculated the coupling constant for "gravitational force". But it is relative to electromagnetic force. As per the standard model, the coupling constants for other three are relative to strong force. "Space-time diameter" equation contains "coupling constant relative to electromagnetic force". We have to change all the coupling constants relative to "electromagnetic force" and can find "space time diameter" for each fundamental force. With this "space time diameter" as per the first equation *i.e.* Equation (1), we can find the value of "Siva's constant "*K*" for all fundamental forces. The same is applicable to the newly introduced fundamental force called "bio force" [6]. Its quantum particle is named as "jeeton" similar to that of a "graviton" as a quantum particle of gravitational force. "Jeeton" is a newly introduced name in this paper. The value of "*K*" for each fundamental force has been calculated and tabulated in **Table 1**.

2.1. Coupling Constant for Gravitation

We have Siva's Grand unification equations [5]

$$cd = K \tag{1}$$

$$cd^2 = Gt_p m \tag{2}$$

$$d_x^4 = 2.116991 \times 10^{-77} \times \alpha_x^3 \tag{3}$$

where d_x is space time diameter of fundamental force and α_x is coupling constant with respect to electromagnetic force.

Once again if we review the calculation for quantum of gravity,

$$d_g^4 = 2.116991 \times 10^{-77} \times \alpha_g^3 \tag{4}$$

where d_g is "space time diameter" of gravity force quantum particle *i.e.* graviton and α_g is coupling constant with respect to electromagnetic quantum particle *i.e.* photon.

2.1.1. Space Time Diameter "d_g" for Gravity

Siva's classical equations for space time [7] after considering final revision (The equation mentioned in the paper [7] has been revised due to the change of

Table 1. Values of Siva's Constant "K" for All Fundamental Forces

S.no	Force	Coupling Constant (α)	Coupling Constant with respect to electromagnetic force (α)	Space-time diameter d (as per equation $d_g^4 = 2.116991\times10^{-77}\times\alpha_g^3$) (mts)	Siva's constant K as per equation $Cd = K$ (sqmts/sec)
1	Strong Force	1	137	2.716253×10^{-18}	8.143122×10^{-10}
2	Electromagnetic Force	$\frac{1}{137}$	1	6.783124×10^{-20}	2.033529×10^{-11}
3	Weak interaction	10^{-6}	1.37×10^{-4}	8.58955×10^{-23}	2.5751×10^{-14}
4	Gravitation	1.016788×10^{-39}	1.393×10^{-37}	$1.5466374059\times10^{-47}$	4.636702×10^{-39}
5	Bio-Force (related to interactions of consciousness)	6.3995777×10^{-40}	$8.7674215287\times10^{-38}$	1.09290816×10^{-47}	$3.276456237\times10^{-39}$

"K" as explained in "Section. 1. introduction". The proof has not been provided here)

$$m = 7.9905778\times10^{-17}\times d^{1/3} \tag{5}$$

$$\gamma d^{8/3} = 1.526087946\times10^{-16} \tag{6}$$

where "m" is the fundamental particle with energy equivalent to mc^2 created by space time of any fundamental force. "d" is diameter of its own space. "γ" is its space time density. Siva's gravity equation can be used for any fundamental force. Here let us consider gravity only for our convenience since "m" is nothing but basic building block of mass.

As per Double relativity Effect [1] [2] [3],

$$Vd = K \tag{7}$$

where "V" is velocity of the body existed due to force of gravity at a point at distance "d" from any observer. "K" is Siva's constant and follows the gravity equation $K = Gt_p\left(\frac{m}{d}\right)$ [4]. It is obvious that velocity of light *i.e.* 2.99792458×10^8 mt/sec is the maximum signal velocity in our conventional four dimensional space time. This space time contains density also. We can compare it with any mass density as explained in Siva's classical space time equations [7].

We have equations for quantum of energy

$$E = h\nu \tag{8}$$

$$E = mc^2 \tag{9}$$

As per Equation (7), "d" will be maximum when "$V = c$". This is the stage of the universe contains a signal velocity "c" and the space time density representing space time diameter d_g.

So the diameter of the universe at diameter of graviton *i.e.* d_g. Mathematically,

$$d_g = d_{ug} = \frac{K}{c} \tag{10}$$

We have Siva's constant "K" as explained in paper [4]

$$K = Gt_p\left(\frac{m}{d}\right) \tag{11}$$

And velocity of light $c = 2.99792458\times10^{8}\ \text{mt/sec}$

$$\therefore d_{ug} = \frac{K}{c} = \frac{Gt_p m}{cd} = \frac{Gt_p \times 7.9905778\times10^{-17}\times\left(d_g\right)^{1/3}}{c\times d}$$

Substitute the following values [11] in it.

$$G = 6.67408\times10^{-11}\,\text{m}^3\cdot\text{kg}^{-1}\cdot\text{sec}^{-2}$$

$$t_p = 5.39116\times10^{-44}\ \text{sec}$$

$$c = 2.99792458\times10^{8}\ \text{m/sec}\quad \text{in}$$

$$m = 7.9905778\times10^{-17}\left(d_{ug}\right)^{1/3}\quad \text{as per Equation (5)}$$

$$d = d_g = d_{ug}$$

$$\therefore d_g = \frac{6.67408\times10^{-11}\times5.39116\times10^{-44}\times7.9905778\times10^{-17}\times d_g^{1/3}}{2.99792458\times10^{8}\times d_{ug}}$$

$$\therefore d_g^{5/3} = 96.009494375\times10^{-80}$$

$$\therefore d_g = 15.466374059\times10^{-48}$$

$$\therefore d_g = 1.5466374059\times10^{-47}\ \text{mts} \tag{12}$$

Therefore the coupling constant for gravity as per Equation (4)

$$d_g^4 = 2.116991\times10^{-77}\times\alpha_g^3 \tag{13}$$

As per Equation (12) space time diameter for gravity space time $d_g = 1.5466374059\times10^{-47}\ \text{mts}$.

Substitute $d_g = 1.5466374059\times10^{-47}$ in Equation (13)

$$\left(1.5466374059\times10^{-47}\right)^4 = 2.116991\times10^{-77}\times\alpha_g^3$$

$$5.7220814849\times10^{-188} = 2.116991\times10^{-77}\times\alpha_g^3$$

$$\alpha_g^3 = \frac{5.7220814849\times10^{-188}}{2.116991\times10^{-77}}$$

$$\alpha_g^3 = 2.7029314177\times10^{-111}$$

$$\alpha_g = 1.39298040988\times10^{-37} \tag{14}$$

Thus as per Equation (14) Coupling constant for gravitational force "α_g" is 1.393×10^{-37}.

Note: in paper [4] the calculation has been done by mistake with space time radius. It must be space time diameter. In this paper it is rectified and the calculation has been revised. It will not affect any other calculations.

2.1.2. Space Time Diameter "d_b" for "Bio Force"

"Bio-force" is a newly introduced fundamental force. It is introduced in the paper [6]. We have to define it from the fundamentals. Bio force is the force whose

presence and absence shows the difference between living and non living things. In "Super theory of relativity" [8] it is explained that consciousness is an effect of bio force in living things [8]. At this stage involvement of "Super theory of Relativity" and "film theory of the universe" clearly defined the terms "observer" and "observation". This concept emphasized the formation of consciousness which is an affect of "bio-force" which is just like other four fundamental forces. As per its conclusions, we cannot avoid the importance of "consciousness" which is the main constituent that differentiates the "living" and "non-living" things of the universe. In order to incorporate "consciousness" in to physics "Super theory of Relativity" [8] has been introduced to physics. Special theory of Relativity explains the transformations between physical objects or frames where as "Super Theory of Relativity" explains the interactions between living things and the physical universe by "Film Theory of the Universe" [8]. As per this concept the universe in which we are living is a result of slide show of films changing in minute fraction of second. There is no link between these films. The events are prefixed and programmed. Universal films are also similar to movie films. All the films are separate. But universe as a whole is a continuous flow of events. The continuity is due to consciousness which is a direct consequence of "bio-force".

We know the maximum signal velocities for "gravity space time" *i.e.* velocity of light "c" and for "bio-force" (source of consciousness) "$\sqrt{2}c$" as per Super theory of relativity [8].

This "classical space time equation" is used to find out the quantum nature of gravity just like other natural forces and emphasized that all natural fundamental forces are outcome of space time density for which "K" is a parameter. In common, all fundamental particles are formed by contraction of their space time and named as a particle called "K-Suryon" [5]. K-Suryon appears as a fundamental particle of concerned force. Thus for Gravity, K-Suryon is graviton. For electromagnetic force, K-Suryon is a photon.

If we consider the same Equations (1)-(3) to the K-Suryon of bio-force but with a signal velocity $\sqrt{2}c$ [6] [8] we can calculate value of Siva's constant "K" for "bio-force".

So equations for quantum of bio-force *i.e.* K-suryon of bio force are

$$\sqrt{2}cd_b = K_b \tag{15}$$

$$K_b = Gt_p\left(\frac{m}{d_b}\right) \tag{16}$$

$$\sqrt{2}cd_b^2 = Gt_p m \tag{17}$$

where d_b is space time diameter and and K_b is siva's constant for bio force particle "jeeton".

We have Equation (5) we can apply it to "bio force" and re write it as

$$m = 7.9905778\times10^{-17}\times d_b^{1/3} \tag{18}$$

$$\sqrt{2}c \times d_b^2 = G \times t_p \times 7.9905778 \times 10^{-17} \times d_b^{1/3}$$

Substitute the following values [11] in (18)

$$G = 6.67408 \times 10^{-11}\,\mathrm{m}^3 \cdot \mathrm{kg}^{-1} \cdot \mathrm{sec}^{-2}$$

$$t_p = 5.39116 \times 10^{-44}\,\mathrm{sec}$$

$$c = 2.99792458 \times 10^8\,\mathrm{m/sec} \quad \text{in}$$

$$m = 7.9905778 \times 10^{-17} \left(d_b\right)^{1/3}$$

$$\therefore d_b = \frac{6.67408 \times 10^{-11} \times 5.39116 \times 10^{-44} \times 7.9905778 \times 10^{-17} \times d_b^{1/3}}{\sqrt{2} \times 2.99792458 \times 10^8 \times d_b}$$

$$\therefore d_b^{5/3} = 67.81349277 \times 10^{-80}$$

$$\therefore d_b = 12.554218 \times 10^{-48}$$

$$\therefore d_b = 1.2554218 \times 10^{-47}\,\mathrm{mts} \tag{19}$$

Similar to Equation (4)

$$d_b^4 = 2.116991 \times 10^{-77} \times \alpha_b^3 \tag{20}$$

As per Equation (19) space time diameter for bio force space time $d_b = 1.2554218 \times 10^{-47}$.

Substitute $d_b = 1.2554218 \times 10^{-47}$ in

$$\left(1.2554218 \times 10^{-47}\right)^4 = 2.116991 \times 10^{-77} \times \alpha_b^3$$

$$2.4840405 \times 10^{-188} = 2.116991 \times 10^{-77} \times \alpha_b^3$$

$$\alpha_b^3 = \frac{2.4840405 \times 10^{-188}}{2.116991 \times 10^{-77}}$$

$$\alpha_b^3 = 1.17338265 \times 10^{-111}$$

$$\alpha_b = 1.05474276 \times 10^{-37} \tag{21}$$

Thus as per (21) Coupling constant for bio force "α_b" is 1.055×10^{-37}.

3. Siva's Constant "*K*" for All Fundamental Forces

As explained in Section 2, Siva's constant "*K*" for each fundamental force has been calculated and tabulated in **Table 1**.

4. Applications of Siva's Constant "*K*" and Space Time Diameter d_x

4.1. Spin & Siva's Constant "*K*"

We have Equation (1) *i.e.* $Cd = k$.

"*d*" varies for each fundamental force. So "*K*" will be different for each fundamental force.

If we take photon, "space time diameter" will exist. But as per special theory of

relativity its space must be zero since it is moving with velocity of light. So due to limitation to its velocity *i.e. c*, reduces its "space time diameter" and finally will be reduced to zero, as per space time equivalence principle [9], at this point it will have time only. And can be converted to time as per the equation

$$t = 1.44224957 \times r^{2/3}$$

where "r" is space time radius. And space time diameter is "d".

The equation can be written as

$$t = 1.44224957 \times (d/2)^{2/3} \tag{22}$$

where "d" is space time diameter.

Thus at velocity of light it will be totally time "t" only. It means, the flow of time inside photon will be there but the duration between two events will be zero (duration will not exist). In other words time can not be divisible inside photon. It is a quantum of electromagnetic force. In all respects it will not be divisible.

Due to the reduction in "d", the value of "K" will be reduced as per the Equation (1) *i.e.* $cd = K$ where "c" is constant.

Again "K" is related to $\hbar$ asper [5] $K = \sqrt{\frac{\hbar G}{c}}$.

If "K" reduces, $\hbar$ will be increased to compensate it.

$\hbar$ is spin related aspect. Thus spin is related to Sivas constant "K".

Physically it means that a quantum particle moves with velocity of light, its space time diameter will be zero but the space time diameter to be existed for that quantum particle will be reduced to zero and the reduction will cause to change its $\hbar$ and the spin is the equivalent effect of its rotation on its own axis as if it will have a space time diameter "d".

4.2. Gravitational Binding Energy with Space Time Diameter "d_g"

Equation for Gravitational binding energy is [12] [13]

$$E_G = \frac{3GM^2}{5R} \tag{23}$$

where G is Newton's Gravitational constant.

"M" is mass of any spherical body.

"R" is radius of that massive body.

Quantum particle of Gravitational field *i.e.* graviton is a K-suryon created by gravity space time. It is the minimum energy which keeps it as gravitational quantum particle. It is equal to a mass "m" and space time diameter "d".

We have Siva's classical equation as per Equation (5)

$$m = 7.9905778 \times 10^{-17} \times d^{1/3}$$

where "m" is mass of any body and "d" is space time diameter.

We can rewrite the Equation (23) with mass "m" and space time diameter "d"

$$E_G = \frac{3Gm^2}{5\left(\frac{d}{2}\right)}$$

$$E_G = \frac{6Gm^2}{5d}$$

Substitute Equation (4) in Equation (23)

$$E_G = \frac{6G\left(7.9905778\times10^{-17}\times d^{\frac{1}{3}}\right)^2}{5d}$$

$$E_G = \frac{6G\left(7.9905778\times10^{-17}\right)^2\times d^{2/3}}{5d}$$

$$E_G = \frac{6\times6.67408\times10^{-11}\times\left(7.9905778\times10^{-17}\right)^2\times d^{2/3}}{5d}$$

$$E_G = \frac{511.362672294\times10^{-45}}{d^{1/3}}$$

We have space time diameter for gravity space time as per (12)

$$d = 1.5466374059\times10^{-47}\,\text{mts}$$

Therefore

$$E_G = \frac{511.362672294\times10^{-45}}{\left(1.5466374059\times10^{-47}\right)^{1/3}}$$

$$E_G = \frac{5.11362672294\times10^{2}\times10^{-45}}{\left(15.466374059\times10^{-48}\right)^{1/3}}$$

$$E_G = \frac{5.11362672294\times10^{2}\times10^{-45}}{\left(15.466374059\right)^{1/3}\times10^{-16}}$$

$$E_G = \frac{5.11362672294\times10^{-43}}{\left(15.466374059\right)^{1/3}\times10^{-16}}$$

$$E_G = \frac{5.11362672294\times10^{-43}}{2.491511158\times10^{-16}}$$

$$E_G = 2.052419755986\times10^{-27}\,\text{Jouls} \tag{24}$$

We have equation for threshold time

$$\tau = \frac{\hbar}{E_G} \tag{25}$$

Substitute values of $\hbar$ as per [11] and E_G as per Equation (24)

$$\tau = \frac{1.0545718\times10^{-34}}{2.052419755986\times10^{-27}}$$

$$\tau = \frac{1.0545718\times10^{-34}}{2.052419755986\times10^{-27}}$$

$$\tau = 5.13818773\times10^{-8}\,\text{sec}$$

4.3. Explanation to Quantum Entanglement and Origin of Consciousness

- We have concluded two fundamental force particles. One is gravitational force particle "graviton" and another is bio force particle "jeeton" and their space time diameters. One represents material object another represents conscious object.
- "Super Theory of Relativity" [8] explains the interactions between living things and the physical universe by "Film Theory of the Universe" [3] as an interaction between "jeeton" and "graviton".
- These two are separate force particles. Consciousness is an effect of interaction between these two particles. "Super Theory of Relativity" is an application of "Double Relativity Effect". Thus "double relativity effect" is a phenomenon explained in terms of "entanglement" for processing of information between "two consecutive films" of "film theory of the universe" [3]. This process is part of "observation" defined by physics. This can be interpreted in quantum information processing. This must obey quantum de coherence while processing. Based on this concept, it is estimated that minimum processing speed of a conscious brain should be 144 qubits per second. This may be useful for the research on "Hard Problem" of consciousness.

5. Conclusions

1) Space time diameters and their coupling constants for "gravitational force", "bio force" have been calculated from the fundamentals by Siva's "grand unification equation".

2) Siva's constant "*K*" for all five fundamental forces has been calculated and tabulated in Table 1.

3) Spin of quantum mechanics has been interpreted with Siva's constant "*K*". It will be used in "mathematical modeling" of consciousness.

4) Threshold frequency or binding energy of "gravity space time" which plays a role in the phenomenon of "observation" has been calculated by its space time diameter.

"Quantum entanglement" has been interpreted as an effect of relativity and consciousness. It is an effect of "entanglement between "bio force particle" *i.e.* "jeeton" and "graviton".

Conflicts of Interest

The author declares no conflicts of interest regarding the publication of this paper.

References

[1] Kodukula, S.P. (2009) Double Relativity Effect & Film Theory of the Universe. ISBN 978-0-557-07712-0, Raleigh, NC, 5-6, 7, 12-38.

[2] Kodukula, S.P. (2013) *IJoART*, **2**.

http://www.ijoart.org/docs/Derivation-of-Sivas-Constant-K-of-Physics.pdf

[3] Kodukula, S.P. (2017) *International Journal of Physics*, **5**, 99-109. http://pubs.sciepub.com/ijp/5/4/1

[4] Kodukula, S.P. (2017) *International Journal of Theoretical and Mathematical Physics*, **7**, 155-158. http://article.sapub.org/10.5923.j.ijtmp.20170706.01.html

[5] Kodukula, S.P. (2018) *Journal of Modern Physics*, **9**, 1179-1194. https://doi.org/10.4236/jmp.2018.96071

[6] Kodukula, S.P. (2016) *International Journal of High Energy Physics*, **3**, 18-24. http://www.sciencepublishinggroup.com/j/ijhep

[7] Kodukula, S.P. (2013) *International Journal of Advancements in Research & Technology*, **2**, 4. http://www.IJoART.org

[8] Kodukula, S.P. (2014) *American Journal of Modern Physics*, **3**, 232-239. http://article.sciencepublishinggroup.com/pdf/10.11648.j.ajmp.20140306.15.pdf

[9] Kodukula, S.P. (2012) *International Journal of Scientific Research and Publications*, **2**, 1-3. http://www.ijsrp.org/research-paper-1012/ijsrp-p1005.pdf

[10] Kodukula, S.P. (2016) *Open Journal of Biophysics*, **6**, 34-37. https://doi.org/10.4236/ojbiphy.2016.62005

[11] Mohr, P.J., Newell, D.B. and Taylor, B.N. (2016) *Journal of Physical and Chemical Reference Data*, **45**, Article ID: 043102.

[12] Chandrasekhar, S. (1939) An Introduction to the Study of Stellar Structure. University of Chicago, Chicago, 101.

[13] Lang, K.R. (1980) Astrophysical Formulae. Springer Verlag, Berlin, 272. https://doi.org/10.1007/978-3-662-21642-2

Journal of Modern Physics, 2019, 10, 477-485
http://www.scirp.org/journal/jmp
ISSN Online: 2153-120X
ISSN Print: 2153-1196

Energy Gap in Saturn's Rings

Andrey Yu Pospelov[1], Vladimir V. Tchernyi[2]

[1]Independent Researcher, Los Angeles, USA
[2]Modern Science Institute at SAIBR, Moscow, Russia
Email: apospelov@hotmail.com, chernyv@bk.ru

How to cite this paper: Pospelov, A.Y. and Tchernyi, V.V. (2019) Energy Gap in Saturn's Rings. *Journal of Modern Physics*, **10**, 477-485.
https://doi.org/10.4236/jmp.2019.104033

Received: February 13, 2019
Accepted: March 23, 2019
Published: March 26, 2019

Abstract

In this article, we consider, based on the super-diamagnetic model, the new problems of Saturn's rings discovered by Cassini, such as: 1) anomalous purity of water ice; 2) Saturn's magnetic field alignment with the planet's rotation axis; 3) "ring rain" of the submicron particles; 4) the deviation in the qualitative composition of the "rain" from the composition of the rings; 5) "dirt" concentrated in the ring gaps; 6) "plateaus" in Saturn's C ring; 7) age of the rings; 8) roll-off in the spectrum of Saturn's rings, and 9) "propellers" in Saturn's A ring. Interpretation of Cassini's observations of spectral roll-off in Saturn's rings in the wavelength range from 100 micrometers to 0.5 mm is given. It was concluded that the substance of the rings could be in the superconducting state. An explanation of the Cassini spectral data is given using the hypothesis of the existence of a superconducting energy gap in the substance of rings.

Keywords

Saturn Rings, Cassini CIRS Interpretation, Super-Diamagnetic Model, Superconducting Energy Gap, Ring Rain, Plateaus and Propellers in Saturn's Rings

1. Introduction

Cassini's research added new puzzles [1] [2] [3] to long-standing problems [4] [5] [6] [7] [8] and, at the same time, reinforced the super-diamagnetic model of Saturn's rings (Table 1). Due to the fact that each problem of Saturn's rings was explained by a few separate models or hadn't explanation at all [9], we chose an approach that would set a single reason for a dozen known problems. We assumed that such a common cause could be the superconducting state of matter in the rings of Saturn. Then, the numerous phenomena, properties, and effects of superconductors entered into battle with the problems and puzzles of Saturn's

Table 1. Possible solutions of the problems of Saturn's rings based on a super-diamagnetic model.

Problems regarding Saturn's rings	Saturn's ring problems explained through superconducting effects
1) Anomalous purity of water ice (99.9 %)	Superconductivity of ice in Saturn's rings [13], Meissner-Ochsenfeld effect [14]
2) The existence of a temperature boundary beyond the asteroid belt, where the planets may have rings	Superconducting transition temperature (T_c)
3) Great flattening of the rings system. Sharp edges and rings discontinuities. Arcs	The phenomenon of expulsion of the superconductors out of the areas with greater density of magnetic flow [15]
4) Fine periodical structure of the Saturn's rings, density waves	The phenomenon of the formation of a periodic structure in a super-diamagnetic liquid film under the influence of normally oriented magnetic field
5) "Ring rain" of the submicron particles	Disappearance of the super-diamagnetic properties of superconducting particles at a greater depth than London's penetration depth of the magnetic field (50 - 500 nm)
6) Forming and development of the "spokes" of Saturn's B ring	Loss of superconductivity due to the critical magnetic field H_c
7) High reflection and low brightness of the ring particles in the radiofrequency range	Critical frequency for the superconductor, above which electromagnetic waves are absorbed, and below which they are completely reflected (10^{11} Hz)
8) The wide band pulse radiation of the rings (20 kHz - 40.2 MHz)	Non-stationary Josephson phenomenon: generation of electromagnetic waves by Josephson's weak links with the parameter 4.83594×10^{14} Hz/V [16]
9) Existence of Kilometric radiation of the Saturn rings ($\nu < 1.2$ MHz)	The electric field appears due to the movement of the superconducting fluid within the magnetic field
10) Color differentiation of Saturn's rings in a small scale	Dependence of the force of magnetic levitation from the volume of superconducting phase in the bulk matter (observed in experiment)
11) Phenomenon of anomalous inversion of reflection of the radio waves with the circular polarization ($\lambda \geq 1$ cm)	Positive charge of the superconducting carriers (protons) [17]
12) Possible distribution of particles by size in Saturn's rings in the radial direction	Dependence of magnetic separation of the superconducting particles by size, and also, strength, extension, and the range of the applied magnetic field [18]
13) The existence of an atmosphere of molecular oxygen around the rings of Saturn	Magnetic levitation of gas molecules due to diamagnetic expulsion forces induced in superconducting particles by molecular magnetic moments (observed in experiment). Flux pinning [19]
14) Saturn's magnetic field alignment with the planet's rotation axis (<0.06˚)	London moment [20]
15) Increasing the purity of the ice in the radial direction from Saturn	The dependence of the force of expulsion of a superconductor from a magnetic field on the volume of the super conducting phase (observed in experiment)
16) "Dirt" concentrated in the ring's gaps	The phenomenon of expulsion of the superconductors out of the areas with greater density of magnetic flow
17) Deviation in the qualitative composition of the "rain" from the composition of the rings [21]	London's penetration depth , flux pinning, super-diamagnetic expulsion
18) "Plateaus" in Saturn's C ring	Tao effect: Electric-field induced formation of superconducting granular balls [22]
19) Age of the rings	London moment, super-diamagnetic expulsion, flux pinning
20) Roll-off in the spectrum (100 μm - 0.5 mm) [23] [24]	Superconducting energy gap (10^{-4} eV - 10^{-3} eV)
21) "Propellers" in Saturn's A ring [25]	Gyromagnetic effect [26], London moment, super-diamagnetic expulsion
22) Origin, dynamics and evolution of the rings	All phenomena above

rings. Moreover, a deeper analysis using spectral studies indicates that the mystery of the nature of rings is hidden in the physical state of the particles of the rings. In our approach, we proceeded on the basis of one hypothesis about the nature of rings to find a solution to as many problems as possible, no matter how fantastic this hypothesis seemed. In the case of Saturn's icy rings, this required overcoming a psychological barrier, since it seems to everyone that eve-

rything is known about the ice that we deal with in everyday life. But the nature of cosmic ice, which was formed under weightless conditions at very low temperatures (~10 K) for a very long time (~1 billion years), has hitherto been unknown.

2. Super-Diamagnetic Model of Saturn's Rings

We have compiled a list of problems for Saturn's rings and a list of effects, properties, and phenomena for superconductors, and then found a match between each of them. This resulted in the super-diamagnetic model of Saturn's rings (Table 1).

The problems of Saturn's rings with numbers 2 - 13, 22 of Table 1 were considered by us in a previous article [10]. The problems with numbers 1, 14 - 21 will be discussed in this article.

3. Discussion of the New Problems Discovered by Cassini

The rings of Saturn, with rotation at a speed of 20 km/s, with a thickness of 10 m, and a total width of the main rings of 2.82×10^8 m can be considered as a flow of super-diamagnetic thin film fluid (with suspended superconducting particles).

Colloidal systems based on superconducting materials may possess a number of unusual properties. These include an anomalously high initial diamagnetic susceptibility, a non-analytical magnetization curve that is capable (in the case of composite suspension) of changing the sign, and dynamic Josephson contacts [11].

3.1. Anomalous Purity of Water Ice in Saturn's rings

The fact that the rings are extremely pure ice (99.9%) remains the number one mystery. According to popular opinion, the reason for such purity may be that they are very young; otherwise they should darken with age due to accumulated dust. The speed of darkening may depend on the influx of dust, and on the total mass and internal dynamics of the rings [12]. The super-diamagnetic model adds a new factor: self-cleaning of the rings due to the Meissner-Ochsenfeld effect and the London penetration depth of the magnetic field. Due to the fact that icy particles are possibly superconducting, they exhibit super-diamagnetism and the Meissner-Ochsenfeld effect. This allows them to remain in their Kepler orbits, while impurities, as well as ice particles with sizes smaller than 1 micron, cease to interact with the magnetic field of the planet and rush to the planet. Such a mechanism may explain the predominance of water ice in the rings of Saturn.

3.2. Saturn's Magnetic Field Alignment with the Planet's Rotation Axis

Based on data collected by Cassini's magnetometer instrument, Saturn's mag-

netic field appears to be surprisingly well-aligned with the planet's rotation axis. The tilt is much smaller than 0.06 degrees—which is the lower limit of the spacecraft's magnetometer. The core of Saturn probably consists of metallic hydrogen and is superconducting. In accordance with the London moment, a rotating superconductor generates a magnetic field whose axis exactly coincides with the axis of rotation.

3.3. "Rain" of the Submicron Particles

The ring rain that Cassini's Ion Neutral Mass Spectrometer caught falling from Saturn's rings into its atmosphere is only about 24 percent water. This is—a major surprise—given that Saturn's ring system is almost entirely water ice. The rest of the ring rain is composed of organic material and other molecules.

The explanation for this is the loss of super-diamagnetism by superconducting ice particles with a size of less than 1 micron, which corresponds to the doubled London depth of penetration of the magnetic field into the superconductor. Ice particles that have lost super-diamagnetism, nevertheless, retain their diamagnetism, which causes them to move along magnetic field lines.

3.4. The Deviation in the Qualitative Composition of the Rain from the Composition of the Rings

Ring rain is highly contaminated with organic matter and other molecules. Water constituted only about 24 percent of the material tumbling from Saturn's ring system into its atmosphere; the rest is methane, carbon monoxide, dinitrogen, ammonia, carbon dioxide and fragments of organic nanoparticles. Remote observations show that Saturn's ring system, on the whole, is almost entirely water ice. Why is ring rain so deprived of water? It turns out that the rain that falls out of rings consisting of 99.9% water ice contains 76% of pollutants. What kind of mechanism is responsible for this filtration? We believe it to be the simultaneous action of three quantum effects: the Meissner-Ochsenfeld effect, flux pinning for icy particles larger than 1 micron, and the penetration of a magnetic field into a superconductor to the London depth for icy particles smaller or equal to 1 micron. At the same time, the above-mentioned effects do not affect the pollutants.

3.5. "Dirt" Concentrated in the Rings Gaps

The presence of dirt in the gaps of the rings is explained within the framework of the super-diamagnetic model by the magnetic field condensing in the gaps due to expulsion of the magnetic field from the rings, where superconducting ice particles are located, and also, due to the paramagnetic properties of cosmic dust, which tend to the concentrations of the magnetic field.

3.6. "Plateaus" in Saturn's C Ring

The bright areas inside the rings, where a large number of particles are concentrated are called plateaus. The plateaus have a fancy striped structure, while the

neighboring regions seem lumpy or have no obvious structure at all. These textures provide information about different ways in which the ring particles are interacting with each other. Cassini data indicates that the plateaus do not necessarily contain more ring material than the C ring at large, but the ring particles in the plateaus may be smaller, enhancing their brightness. The task of how plateaus are created and maintained has not been solved. The super-diamagnetic model offers a possible solution. When a strong electric field (0.8 kV/mm) is applied to a suspension of micron-sized superconducting particles, the particles quickly aggregate together, to form millimeter-sized balls. The balls contain more than 10^6 particles each. This phenomenon is the result of the interaction between Cooper pairs and a strong electric field. The strong electric field induces surface charges on the particle surface. When the applied electric field is strong enough, Cooper pairs near the surface are depleted, leading to positive surface energy. The minimization of this surface energy leads to aggregation of particles with the formation of balls. If superconducting particles are in a strong electric field and a moderate magnetic field, the electric-field induced balls align in the magnetic-field direction to form ball chains [27].

3.7. Age of the Rings

Estimation of the age of Saturn's rings using a super-diamagnetic model does not depend on the mass of the rings and the extent of their contamination. The estimation is based on the assumption of the origin of the rings from the proto-planetary cloud and the proto-ring disc at occurrence of a magnetic field. Superconducting particles, which were present in the proto-planetary cloud, under the influence of a rotating planetary magnetic field, were involved in a circular rotation. Then they formed into a proto-ring disk due to the effect of super-diamagnetic expulsion and drift into the plane of the magnetic equator, where the magnetic flux density is the smallest. Here, the superconducting particles finally became fixed due to the effect of flux pinning. Flux pinning is the phenomenon where a superconductor is pinned in space by a magnetic field. The flux tubes are pinned in place and cannot move. This pinning is what holds the superconductor in place thereby allowing it to levitate. Time became powerless in destroying the rings. The super-diamagnetic model estimates the age of the rings to be equal to the age of Saturn. Rings began to form with the advent of Saturn's magnetic field.

3.8. Cassini CIRS Data Interpretation

Cassini Composite Infrared Spectrometer (CIRS) spatially resolved Saturn's main rings in the far-infrared, measuring the spectrum from 20 to 400 wavenumbers (cm^{-1}) (between 100 microns and 0.5 mm). A spectral roll-off below 50 cm^{-1} (200 μm) for each of the A, B and C rings was found (**Figure 1**). From these data temperatures and emissivities for each ring were derived. Interpretation of Cassini CIRS spectral roll-off in Saturn's rings has encountered difficulties. The

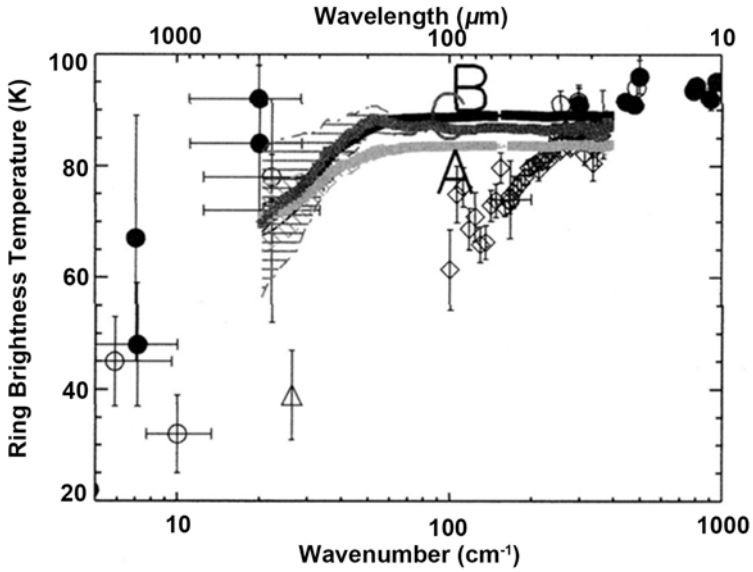

Figure 1. Brightness temperatures of the A, B and C rings as a function of wavenumber (and wavelength).

roll-off in temperature measured by CIRS is principally due to material properties of the ring particles that change dramatically in this region [28]. Lack of laboratory data in the far infrared region below 100 cm^{-1} for water ice analogs of Saturn's rings still hamper the interpretation and understanding of the spectral roll-off observed by the Cassini CIRS instrument [29].

3.8.1. Superconducting Energy Gap

To prove that a substance is a superconductor, it is necessary to measure its energy gap. Cassini CIRS received data in a submillimeter range could be used for the purpose of measuring an energy gap.

If the energy of the infrared radiation is above a certain threshold value, the superconductors absorb radiation very effectively, but if it is below the threshold value then they do not. This is very good evidence that the carriers in a superconductor behave as if they do have an energy gap. The idea of a Cooper pair offers a way of understanding this. Since the pairs are bound, it takes a certain amount of energy, called binding energy, to break the pairs up and this leads to what is known as the superconducting gap. In a superconductor, nothing will happen until an amount of energy equal to the binding energy is supplied. And, once that gap has been bridged, then that energy can be absorbed. This effect can be measured by looking at the way in which superconductors reflect electromagnetic waves; if the waves have an energy (determined by their frequency) which is smaller than the gap energy, the waves are not absorbed and reflect straight back from the superconductor; however, as soon as the energy is large enough, superconducting pairs can be broken apart and energy is absorbed [30].

Ice provides a good example of electrical conduction by proton transfer [31]. Protons, and not just electrons, can travel unobstructed through superconductors. As protons are much heavier than electrons, the pairing of protons is less

likely to be destroyed by high temperatures than the pairing of electrons.

3.8.2. Interpretation of Cassini CIRS Spectral Roll-Off

The super-diamagnetic model of Saturn's rings offers an interpretation for Cassini CIRS observations of a roll-off in Saturn's ring spectra at submillimeter wavelengths. The observed roll-off in the spectrum of the rings is possibly related to the superconducting state of ice. In this case, the thermal conductivity of ice decreases, because charge carriers no longer interact with the lattice and cannot exchange energy, and therefore, they cannot transfer heat from one part of ice to another [32]. The steepness in the curve in **Figure 1** can be interpreted using the two-fluid model of a superconductor, where fewer and fewer normal protons participate in heat transfer with increasing ring radiation wavelengths and more and more superconducting protons do not participate in heat transfer.

It can be assumed that the ice of the Saturn ring is a high-temperature proton superconductor with an energy gap of $2\Delta = 6.2 \times 10^{-3}$ eV (which corresponds to 200 μm) and a superconducting transition temperature T_c of at least 100 K. With such values of 2Δ and T_c, the **Equation 1** for the width of the superconducting energy gap for ice in the rings of Saturn takes the form:

$$2\Delta = 3/5 k_B T_c. \tag{1}$$

where k_B is Boltzmann constant.

3.9. "Propellers" in Saturn's a Ring

The propellers are gaps in the ring material which were created by a moonlets. These moonlets are smaller than known moons but larger than the particles making up Saturn's rings. It is estimated that these moonlets could number in the millions.

The reason for this phenomenon may be a gyromagnetic effect which takes place when a magnetic field is applied to a superconducting body (moonlet). Then superconductor acquires an angular moment in direction opposite to the applied field and it starts to spin spontaneously. Due to the London moment, a rotating superconductor (moonlet) generates its own magnetic field, which in turn, moves superconducting particles apart, forming double-armed propeller structures.

4. Conclusions

The interpretation of Cassini data is particularly relevant now after the recent completion of the mission (2017). Especially important is the analysis of the physical characteristics of the particles of the rings because behind them there lies the nature of the substance of the rings. Such information is contained in an unexpected drop in the spectral range of sub-millimeter waves. Classical approaches to the problem do not give satisfactory results. Our approach to using the super-diamagnetic model of Saturn's rings, based on the assumption of the superconducting nature of the substance of the rings, is new, timely, and leading

to far reaching consequences.

For example, conclusions from the presented work can be extended to the rings of other objects of the Solar System such as the rings of Jupiter, Uranus, Neptune, minor planets and centaurs Chariklo and Charon, and possible ring system around Rhea, which at least partially composed of water ice and possibly other superconducting substances. As a result, it can also be argued that Chariklo, Charon and Rhea have their own magnetic fields.

Conflicts of Interest

The authors declare no conflicts of interest regarding the publication of this paper.

References

[1] Gary, S. (2010) Saturn's Rings a Chaotic Clatter. News in Science. http://www.abc.net.au/science/articles/2010/03/19/2849841.htm

[2] News (2018) Groundbreaking Science Emerges from Ultra-Close Orbits of Saturn. JPL, Caltech. https://www.jpl.nasa.gov/news/news.php?feature=7251

[3] Mission News (2004) Cassini Exposes Puzzles about Ingredients in Saturn's Rings. Cassini, NASA. https://www.nasa.gov/mission_pages/cassini/media/cassini-070204.html

[4] Safronov, V.S. (1969) Evolution of Protoplanet Cloud and Formation of the Earth and Planets. Nauka (Russian), Moscow.

[5] Esposito, L.W., Cuzzi, J.N., Holberg, J.B., Marouf, E.A., Tyler, G.L. and Porco, C.C. (1984) Saturn's Rings, Structure, Dynamics and Particle Properties. In: Gehrels, T. and Mattews, M.S., Eds., *Saturn*, Univ. Arizona Press, Tucson, 463-545.

[6] Jones, G.H., Krupp, N., Kruger, H., Roussos, E., Ip, W.-Y., Mitchell, D.G., Krimigis, S.M., Woch, J., Lagg, A., Franz, M., Dougherty, M.K., Arridge, C.S. and McAndrews, H.J. (2006) *Geophysical Research Letters*, **33**, L21202. https://doi.org/10.1029/2006GL028146

[7] Goldstein, R.M. and Morris, G.A. (1973) *Icarus*, **20**, 249. https://doi.org/10.1016/0019-1035(73)90002-X

[8] (2005) Saturn's Rings Have Own Atmosphere. ESA, Cassini-Huygens. https://www.esa.int/Our_Activities/Space_Science/Cassini-Huygens/Saturn_s_rings_have_own_atmosphere

[9] NASA Science, Solar System Exploration (2017) Plateaus up Close. Photojournal: PIA20529. https://solarsystem.nasa.gov/resources/17638/plateaus-up-close/

[10] Tchernyi, V.V. and Pospelov, A.Yu. (2007) *Astrophysics and Space Science*, **307**, 347-356. https://doi.org/10.1007/s10509-006-9054-7

[11] Kalikmanov, V.I. and Dyadkin, I.G. (1989) *Journal of Physics*: *Condensed Matter*, **1**, 993-997. https://doi.org/10.1088/0953-8984/1/5/015

[12] Redd, N.T. (2017) Cassini's "Grand Finale" Could Solve Saturn's Lingering Mysteries. Scientific American.

[13] Babushkin, A.N., Kobelev, L.Ya. and Babushkina, G.V. (2006) *High Pressure Research*, **3**, 165-167. https://doi.org/10.1080/08957959008246064

[14] Tinkham, M. (2004) Introduction to Superconductivity. 2nd Edition, Dover Publication, Mineola, New York.

[15] Blums, E.S., Cebers, A.O. and Maiorov, M.M. (1997) Magnetic Fluids. Berlin.

[16] Kalikmanov, V.I. and Diad'kin, I.G. (1987) Superdiamagnetic Fluids. Pisma v Zhurnal Tekhnischeskoi Fiziki.

[17] Mullins, J. (2005) Superconductors Have No Need to Be Negative. New Scientist, 16. https://www.newscientist.com/.../mg18624984-400-superconductors-have-no-need-to

[18] Barsoum, M. (1988) Magnetic Separation of High T_c Powders. *Proceedings of the Superconductor Symposium*, 90*th Annual Meeting of American Ceramic Society*, Westerville, 1-5 May 1988, 554-562.

[19] Flux Pinning—Wikipedia. https://en.wikipedia.org/wiki/Flux_pinning

[20] London Moment—Wikipedia. https://en.wikipedia.org/wiki/London_moment

[21] Temming, M. (2018) Saturn's "Ring Rain" Is a Surprising Cocktail of Chemicals. Science News.

[22] Tao, R., Xu, X. and Lan, Y.C. (2002) *International Journal of Modern Physics B*, **16**, 2529-2535. https://doi.org/10.1142/S021797920201261X

[23] Spilker, L.J., Pilorz, S.H., Wallis, B., Edgington, S.G., Brooks, S., Pearl, J. and Flasar, F.M. (2005) Saturn Ring Temperature Roll-Off at Submillimeter Wavelengths from Cassini CIRS Observations. AGU Spring Meeting Abstracts. http://adsabs.harvard.edu/abs/2005AGUSM.P13A..05S

[24] Spilker, L.J., Pilorz, S.H., Edgington, S.G., Wallis, B.D., Brooks, S.M., Pearl, J.S. and Flasar, F.M. (2005) *Earth Moon and Planets*, **96**, 149-163. https://doi.org/10.1007/s11038-005-9060-8

[25] Chow, D. (2010) Giant Propellers Discovered in Saturn's Rings. Science & Astronomy, July 08, 2010.

[26] Hirsch, J.E. (2018) Spinning Superconductors and Ferromagnets. *Acta Physica Polonica A*, **133**, 350-355. https://doi.org/10.12693/APhysPolA.133.350

[27] Tao, R., Xu, X. and Amr, E. (2003) *Physics C*: *Superconductivity*, **398**, 78-84. https://doi.org/10.1016/j.physc.2003.09.069

[28] Nugent, C.R., Spilker, L.J., Edgington, S.G., Russell, C.T., Pilorz, S.H., Altobelli, N. and Gudipati, M. (2007) Investigating the Composition of Saturn's Rings Using Cassini CIRS Data. AGU Fall Meeting Abstracts. https://www.researchgate.net/publication/253390914_Investigating_the_Composition_of_Saturn's_Rings_Using_Cassini_CIRS_Data

[29] Gudipati, M.S. (2009) Laboratory Studies for Planetary Sciences. A Planetary Decadal Survey White Paper Prepared by the American Astronomical Society (AAS) Working Group on Laboratory Astrophysics (WGLA). https://www.researchgate.net/publication/45876087_Laboratory_Studies_for_Planetary_Sciences_A_Planetary_Decadal_Survey_White_Paper_Prepared_by_the_American_Astronomical_Society_AAS_Working_Group_on_Laboratory_Astrophysics_WGLA

[30] Blundell, S.J. (2009) Superconductivity: A Very Short Introduction (Very Short Introductions). OUP Oxford, Kindle Edition, 59. https://doi.org/10.1093/actrade/9780199540907.001.0001

[31] Bradley, R.S. (1957) *Transactions of the Faradey Society*, **53**, 687.

[32] Rose-Innes, A.C. and Rhoderick, E.H. (1978) Introduction to Superconductivity. 2nd Edition, International Series in Solid State Physics.

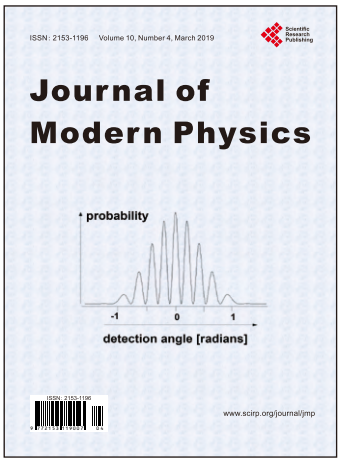

Call for Papers

Journal of Modern Physics

ISSN: 2153-1196 (Print) ISSN: 2153-120X (Online)
http://www.scirp.org/journal/jmp

Journal of Modern Physics **(JMP)** is an international journal dedicated to the latest advancement of modern physics. The goal of this journal is to provide a platform for scientists and academicians all over the world to promote, share, and discuss various new issues and developments in different areas of modern physics.

Editor-in-Chief

Prof. Yang-Hui He City University, UK

Subject Coverage

Journal of Modern Physics publishes original papers including but not limited to the following fields:

Biophysics and Medical Physics
Complex Systems Physics
Computational Physics
Condensed Matter Physics
Cosmology and Early Universe
Earth and Planetary Sciences
General Relativity
High Energy Astrophysics
High Energy/Accelerator Physics
Instrumentation and Measurement
Interdisciplinary Physics
Materials Sciences and Technology
Mathematical Physics
Mechanical Response of Solids and Structures
New Materials: Micro and Nano-Mechanics and Homogeneization
Non-Equilibrium Thermodynamics and Statistical Mechanics
Nuclear Science and Engineering
Optics
Physics of Nanostructures
Plasma Physics
Quantum Mechanical Developments
Quantum Theory
Relativistic Astrophysics
String Theory
Superconducting Physics
Theoretical High Energy Physics
Thermology

We are also interested in: 1) Short Reports—2-5 page papers where an author can either present an idea with theoretical background but has not yet completed the research needed for a complete paper or preliminary data; 2) Book Reviews—Comments and critiques.

Notes for Intending Authors

Submitted papers should not have been previously published nor be currently under consideration for publication elsewhere. Paper submission will be handled electronically through the website. All papers are refereed through a peer review process. For more details about the submissions, please access the website.

Website and E-Mail

http://www.scirp.org/journal/jmp **E-mail: jmp@scirp.org**

What is SCIRP?

Scientific Research Publishing (SCIRP) is one of the largest Open Access journal publishers. It is currently publishing more than 200 open access, online, peer-reviewed journals covering a wide range of academic disciplines. SCIRP serves the worldwide academic communities and contributes to the progress and application of science with its publication.

What is Open Access?

All original research papers published by SCIRP are made freely and permanently accessible online immediately upon publication. To be able to provide open access journals, SCIRP defrays operation costs from authors and subscription charges only for its printed version. Open access publishing allows an immediate, worldwide, barrier-free, open access to the full text of research papers, which is in the best interests of the scientific community.

- High visibility for maximum global exposure with open access publishing model
- Rigorous peer review of research papers
- Prompt faster publication with less cost
- Guaranteed targeted, multidisciplinary audience

Scientific Research Publishing

Website: http://www.scirp.org

Subscription: sub@scirp.org

Advertisement: service@scirp.org